



저작자표시-비영리-변경금지 2.0 대한민국

이용자는 아래의 조건을 따르는 경우에 한하여 자유롭게

- 이 저작물을 복제, 배포, 전송, 전시, 공연 및 방송할 수 있습니다.

다음과 같은 조건을 따라야 합니다:



저작자표시. 귀하는 원저작자를 표시하여야 합니다.



비영리. 귀하는 이 저작물을 영리 목적으로 이용할 수 없습니다.



변경금지. 귀하는 이 저작물을 개작, 변형 또는 가공할 수 없습니다.

- 귀하는, 이 저작물의 재이용이나 배포의 경우, 이 저작물에 적용된 이용허락조건을 명확하게 나타내어야 합니다.
- 저작권자로부터 별도의 허가를 받으면 이러한 조건들은 적용되지 않습니다.

저작권법에 따른 이용자의 권리는 위의 내용에 의하여 영향을 받지 않습니다.

이것은 [이용허락규약\(Legal Code\)](#)을 이해하기 쉽게 요약한 것입니다.

[Disclaimer](#)

Ph.D. Dissertation of Engineering

Development and Clinical Application of the Encoded Bead- Based Multiplex Assay Platform

코드화된 비드 기반 다중 분석 플랫폼의
개발 및 임상 적용

August 2023

Graduate School of
Electrical and Computer Engineering
Seoul National University
Bioengineering Major

Hunjong Na

Development and Clinical Application of the Encoded Bead- Based Multiplex Assay Platform

지도 교수 권 성 훈

이 논문을 공학박사 학위논문으로 제출함
2023 년 8 월

서울대학교 대학원
전기컴퓨터공학부
나 훈 중

나훈중의 공학박사 학위논문을 인준함
2023 년 8 월

위 원 장	<u>이 정 찬</u>	(인)
부위원장	<u>권 성 훈</u>	(인)
위 원	<u>박 옥</u>	(인)
위 원	<u>최 정 일</u>	(인)
위 원	<u>장 지 성</u>	(인)

Abstract

The same symptoms may come from various diseases. Therefore, many diagnoses are performed using biomarkers in blood, sputum, urine, and cerebrospinal fluid (CSF). Compared to single analysis methods such as enzyme-linked immunosorbent assay (ELISA), multiplex diagnosis can improve workflow and save patient samples, reagents, consumables, and test time. In particular, the advantage of reducing the amount of patient samples is that it can increase test accessibility by reducing the burden of sample collection in addition to financial benefits. Furthermore, the high accuracy obtained by combining multiple biomarkers can increase the possibility of early diagnosis through routine tests.

In a multiplex assay platform using coded beads, different probes are attached according to the code assigned to the beads and hundreds or thousands of beads are mixed and reacted with patient samples. By checking the code of beads, i.e. the type of probe, various biomarker information can be obtained. Although the concept of the technology had been proven before my joining, it was insufficient for use in actual diagnostic markets due to a lack of production volume, variation in performance, and lack of programs to analyze codes of beads. This dissertation describes the development process of the encoded bead-based multiplex assay platform to a level that can be used for actual diagnosis. Also, the results applied to Alzheimer's dementia (AD) using the developed platform are described.

In order to easily handle beads and reduce variations, it is necessary to impart magnetism to beads. However, commercial magnetic particles have ferromagnetism that retains a magnetism

even in the absence of external magnetic fields. These magnetic particles form large lumps, and cannot make beads in uniform shape. To solve this problem, I developed a method for mass-synthesizing superparamagnetic nanoparticles.

A system had been developed that can produce beads of a desired shape by illuminating ultraviolet rays reflected by a micro-mirror array onto a UV-curable polymer. This system has the advantage of providing various shapes of beads in real-time, but for using beads in actual diagnostic sites, it is necessary to develop a system capable of producing millions of beads within a short time. To increase production volume, I introduced a large-area exposure system used in semiconductor processes and solved problems arising from differences between photoresists used in semiconductors and polymers. As a result, I can increase the production capacity to 3.5 million per hour.

In order to couple biomarkers on beads, suitable functional groups must be created on the surface of beads. In this dissertation, encoded beads were made by patterned UV and then coated with silica to increase stability. After that, amine and carboxylic acid were sequentially made on the surface of the beads. When amine modification was performed using commonly used material, performance variations occurred due to randomness during the reaction process and hydrolysis during the storage stage. To solve this problem, I introduced alternative material and optimized protocols utilizing its characteristics, and the variation in performance was reduced to less than 5%. I also developed a strategy for effectively assigning codes to beads, an automatic imaging device, and a decoding algorithm.

I performed a comparative evaluation between the developed

platform and the conventional method. The beads can be pre-coupled with probes in large quantities and used for long periods while ELISA requires attaching probes every test. The probe material required for one test can be saved about 100 times. When assuming testing ten biomarkers, the amounts of sample, antibody, fluorescent, and buffers were reduced in the developed multiplex platform by 30, 3, 20, and 15 times, respectively. Also, reaction time was halved due to the beads acting as a 3D suspension array.

The developed platform has been applied to various clinics such as human papillomavirus (HPV), sexually transmitted infections (STIs), tuberculosis, sepsis, and Alzheimer's disease (AD). This dissertation describes the application to dementia. Related biomarkers are changed decades before the onset of dementia. If these changes in biomarkers are detected in advance, the onset of dementia can be significantly delayed through treatment. The methods for diagnosing dementia are neuropsychological test, CSF check, and positron emission tomography (PET) imaging. A neuropsychological test is not possible for early diagnosis, and a CSF check is not suitable for routine tests due to the difficulty in collecting samples. PET imaging also has low accessibility due to its high cost. In this dissertation, I showed that dementia diagnosis is possible with about 80% accuracy by measuring multiple blood biomarkers and algorithmizing them.

Keyword: multiplex, encoded bead, surface functionalization, image processing, clinical application, Alzheimer's disease

Student Number: 2013-30964

Table of Contents

Chapter 1. Introduction.....	1
1.1. Needs for multiplex assay technology.....	1
1.2. Other multiplex assay technologies.....	5
1.3. Previous research in the group.....	7
Chapter 2. Platform development.....	10
2.1. Synthesis of superparamagnetic nanoparticle.....	11
2.2. Implementation of optical setup for mass production.....	13
2.3. Solving cracks of silica layer.....	20
2.4. Functionalize the surface of the bead.....	24
2.5. Development of coding scheme and decoding program.....	29
2.6. Overall procedure to use QMAP™.....	32
2.7. Efficiency comparison between ELISA and QMAP™.....	34
Chapter 3. Clinical applications in Alzheimer' s disease (AD)....	38
3.1. Advantages of blood-based diagnosis in AD.....	39
3.2. Development of QPLEX™ Alz plus assay kit.....	41
3.3. Apply to the other independent cohort.....	44
3.4. Improvement of the kit using additional biomarker.....	46

Chapter 4. Conclusion and Discussion.....	48
4.1. Summary of dissertation.....	49
4.2. Comparison with the other commercialized technology	50
4.3. Limit of the platform.....	52
4.4 Future work	54
Bibliography	56
Abstract in Korean	63

Chapter 1. Introduction

1.1. Needs for multiplex assay technology

Personalized medicine, also referred to as precision medicine, is a medical model that separates people into different groups based on their predicted response or risk of disease. It is difficult to accurately determine which disease an individual has based solely on the symptoms they experience. For example, symptoms such as fever, headache, lethargy, and muscle pain are common to many diseases, including respiratory diseases, gastrointestinal diseases, influenza, and meningitis. Medical decisions, practices, interventions, and/or products must be tailored to the individual patient. The goal of personalized medicine is to provide the most suitable medicine, at the right dose, for the right person, at the right time, at a reasonable cost[1]. Personalized medicine can be used in various ways to facilitate disease prevention, diagnosis, and treatment. Diagnostic testing is often employed for selecting appropriate and optimal therapies based on the context of a patient' s genetic content or other molecular or cellular analysis[2].

Even within the same disease, there can be various variations depending on the mutation. For example, human immunodeficiency viruses (HIV) has more than 60 variations, and sexually transmitted infections (STIs), human papillomavirus (HPV) infection, and influenza each have more than a dozen variations[3,4]. Recently, many mutations have also been occurred in coronavirus disease 2019 (COVID-19), causing us great suffering. There are various variations even in one disease, so there are limitations in diagnosing them separately. Furthermore, in the case of sepsis and tuberculosis, there are dozens of causative pathogen, and to determine antibiotic resistance according to mutation, it is necessary to diagnose using a multiplex platform.

Another advantage of diagnosis based on multiple biomarkers is that they show higher accuracy than diagnoses using a single biomarker. In the diagnosis of prostate cancer, using only a single

biomarker shows an accuracy of 70%, but combining 5 biomarkers can increase the accuracy to 99% [5]. In the case of celiac disease, using a single biomarker for diagnosis showed a sensitivity of about 40%, but combining these three biomarkers increased the sensitivity to 80% [6].

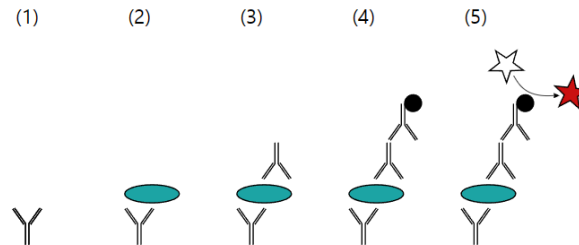


Figure 1. A sandwich ELISA. (1) Plate is coated with a capture antibody; (2) sample is added, and any antigen present binds to capture antibody; (3) detecting antibody is added, and binds to antigen; (4) enzyme-linked secondary antibody is added, and binds to detecting antibody; (5) substrate is added, and is converted by enzyme into a detectable form [7].

Multiplex assays have gained popularity for their advantages of saving sample volume and time by improving workflows when compared to assays that measure a single analyte, such as enzyme-linked immunosorbent assay (ELISA). ELISA is a commonly used analytical biochemistry assay that uses antibodies and color change to detect the presence of a ligand (commonly a protein) in a liquid sample [8]. In ELISA, antigens from the sample to be tested are attached to a surface where a matching capture antibody is pre-coated. Then, a matching detection antibody is applied over the surface so it can bind to the antigen. Detection antibody is linked to an enzyme and then any unbound antibodies are removed. In the final step, a substance containing the enzyme's substrate is added. If there was binding, the subsequent reaction produces a detectable signal, most commonly a color change (Figure 1). ELISA is typically performed on a 96-well plate. The tester knows which capture probe is coated in each well, so they can determine which type and how much of a biomarker the patient has based on the location of the well where the color changes and the degree of color change. Due to the nature of ELISA,

which checks for color change in the well's internal solution, only one type of probe can be used in one well. If multiple biomarkers are to be checked, and if 96 types of biomarkers are to be checked in extreme cases, all 96 wells must be used to diagnose one patient. In other words, it requires intensive labor and typically shows intra- and inter-assay variability [9].

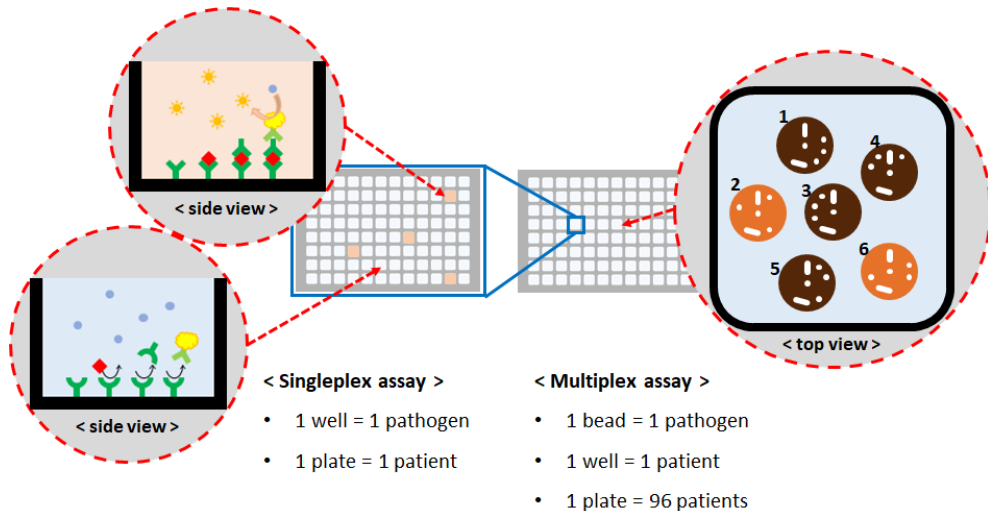


Figure 2. Comparison between ELISA and bead-based multiplex.

In contrast, in the encoded bead-based multiplex assay, the subject of this dissertation, can diagnose much more efficiently. The encoded bead-based multiplex assay is a type of multiplex assay that uses beads to simultaneously measure multiple analytes in a single experiment. Each type of bead is uniquely encoded to distinguish one type from another. In an encoded bead-based multiplex assay, different probes are coated onto beads according to codes. Beads with various codes are then mixed and injected into a well, allowing for the simultaneous detection of multiple biomarkers in a single well. The beads can be injected into one well up to 5,000 beads. In other words, even if 50 beads are used per code, 100 types of biomarkers can be checked in one well. If all 96 wells are used, 96 patients can be diagnosed, making it nearly 100 times more efficient than ELISA (Figure 2).

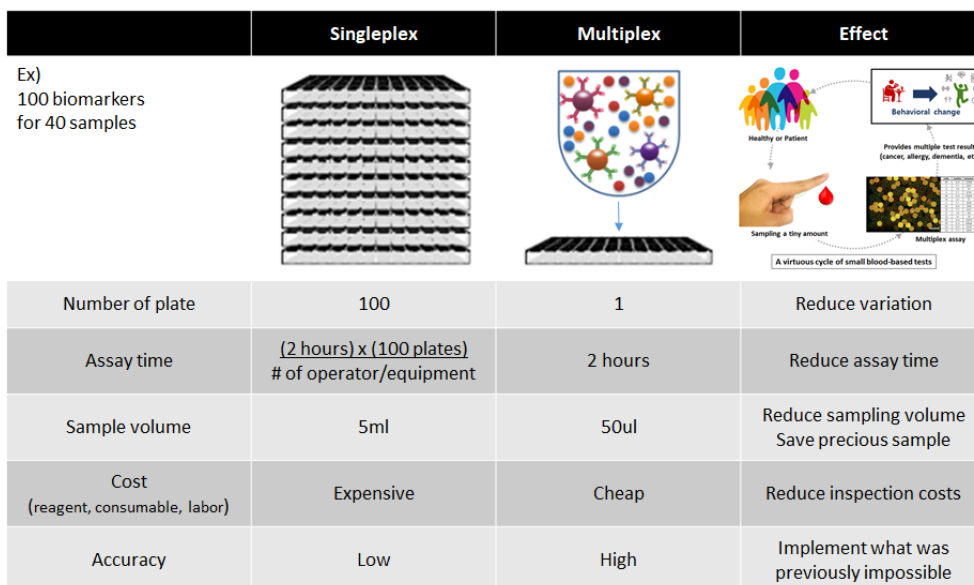


Figure 3. Comparison of theoretical differences between ELISA and multiplex assay assuming a case where 100 biomarkers are tested for 40 patients.

Figure 3 is a comparison table between ELISA and multiplex assay assuming a case where 100 biomarkers are tested for 40 patients. This assumption is to match the common ELISA protocol. In ELISA, an antigen with a known concentration is serially diluted to draw a standard curve for quantification, and typically 16-wells are used for duplication of 8 concentrations. The remaining 80-wells are allocated for duplication of 40 samples to reduce assay error. The signal of the sample well and the signal of the standard curve are compared to calculate how much biomarker is present in the patient's sample. In the previous paragraph, an example of testing multiple types of pathogens in one 96-well plate was given to explain the difference in principle with multiplex assay, but generally one type of pathogen is tested in one plate and the number of plates increases depending on the number of pathogens to be tested. In a situation where 100 biomarkers are tested, there is a 100-fold difference in the number of plates required. This 100-fold includes not only the number of plates but also labor, pipette tips, reagents and other parts that differ by 100-fold. Multiplex assays have several advantages over traditional assays,

including reduced sample volume requirements, faster analysis times, and improved workflow efficiency.

Especially important is the difference in sample volume. Samples such as urine or sputum can be easily obtained in large quantities, but blood or cerebrospinal fluid can be difficult to obtain in large quantities or painful to obtain. Being able to save such precious samples means more than just monetary gain. Also, if less sample is needed for testing, there is no need to sample a large amount, and by sampling only a small amount of blood from the fingertip like a diabetes test, practical and psychological hurdles can be greatly reduced. If testing is possible with a small sample and the cost of testing is low and combined with high accuracy of multiple diagnoses, early diagnosis through light and routine tests becomes possible.

1.2. Other multiplex assay technologies

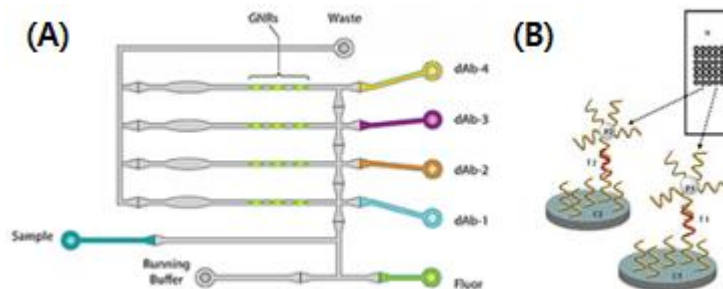


Figure 4. Other multiplex technologies. (A) Microfluidics. (B) Microarray [10,11].

There are several representative technologies for implementing multiplex diagnosis, including microfluidics, microarray, and encoded-bead methods. Microfluidics refers to the manipulation of small volumes of fluids (usually in the range of microliters to picoliters) using channels with dimensions of tens to hundreds of micrometers. In a microfluidics-based multiplex assay, multiple microfluidic channels are created and each channel is coated with a different probe. The patient's sample is then flowed through the

multiple channels simultaneously and the location of the probe-reactive channels can be used to determine which biomarkers the patient has [12]. A microarray is a two-dimensional array on a solid substrate that assays large amounts of biological material using high-throughput screening miniaturized, multiplexed and parallel processing and detection methods [13–15]. In a microarray-based multiplex assay, probes are spotted onto the microarray substrate in a precise pattern [16]. The patient's sample is then applied to the microarray and the location of probe-reactive spots can be used to determine which biomarkers the patient has. These multiplex assays also have similar advantages to bead-based multiplex assay compare to traditional assays: reduced sample volume requirements, faster analysis times, and improved workflow efficiency [17].

There are two reasons why I focused on bead-based multiplex technology among these three methods. First, multiplex platforms using microfluidics or microarray have limitations in implementing high plex due to manufacturing technology and spatial constraints. On the other hand, bead-based multiplex platforms can use up to 5,000 beads at once in a space about the size of one well of a 96-well plate because each bead is only a few micrometers in size. Second, even if products are manufactured with the same equipment and protocol, unavoidable variations will occur. Fortunately, in bead technology, millions of beads produced in one reaction chamber can guarantee completely identical performance between them. When a quality control (QC) test is performed by sampling some beads after bead production to check if the product has been manufactured normally, the performance between the QC-used beads and the remaining beads is guaranteed to be identical because they are identical. If it passes QC, you can trust and use it. On the other hand, microfluidics or microarray products are individually manufactured so it is impossible to guarantee that the performance between products used for QC by sampling and remaining products is identical and you can only hope that the frequency of defective products is low.

1.3. Previous research in the group

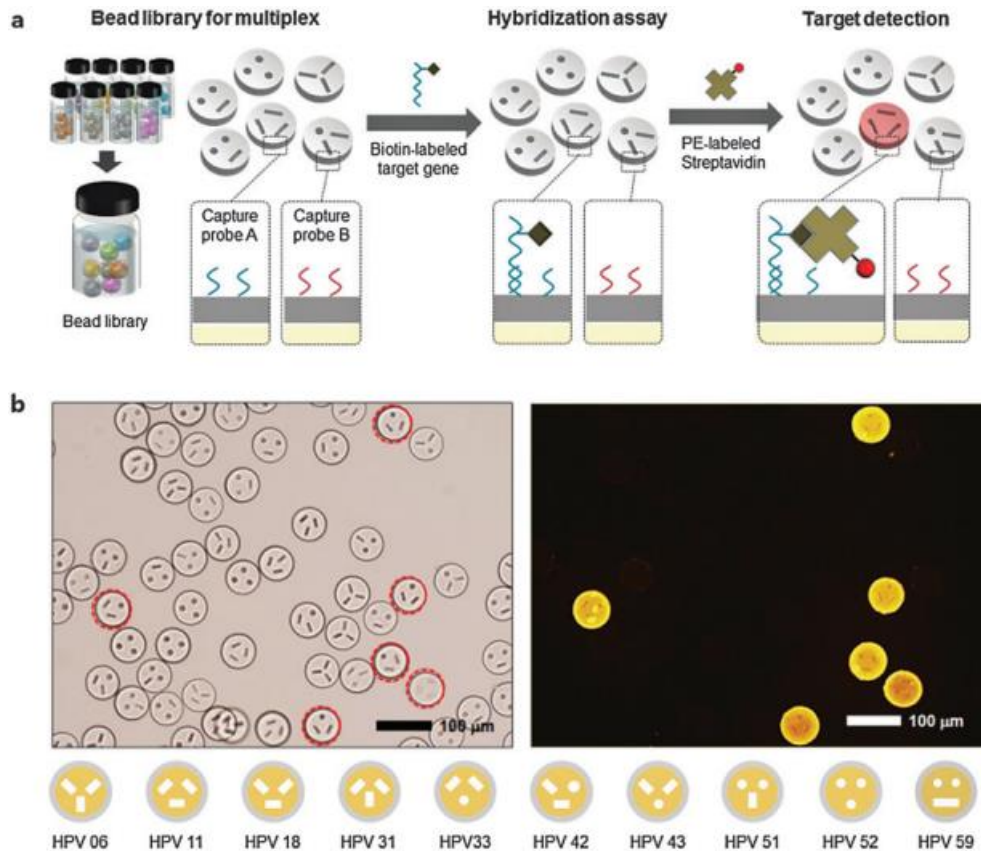


Figure 5. Multiplexed HPV genotyping using encoded silica beads. (a) A conceptual overview of multiplexed HPV genotyping using encoded silica beads. (b) A bright-field and a fluorescence microscopy image after the hybridization assay. Only particles with probes complementary to the target HPV 33 sequences showed strong fluorescence [18].

When I joined the lab, proof of concept for encoded bead-based multiplex technology was already in place. When UV light is shot onto a polymer that reacts with UV light to undergo photopolymerization using a micro mirror array for patterning UV light, the polymer polymerizes into a shape similar to that of UV pattern and beads are formed [19]. During photopolymerization, the desired code can be encoded by adjusting UV pattern. Then coat with silica layer to improve physical and chemical durability of

polymer scaffold and chemically modify bead surface so that probes such as deoxyribonucleic acid (DNA) or protein can be coupled. After coupling different probes according to code, the beads were reacted with variously synthesized HPV sequences at once. As a result, only signal came out from bead with code matching injected DNA species (Figure 5) [18].

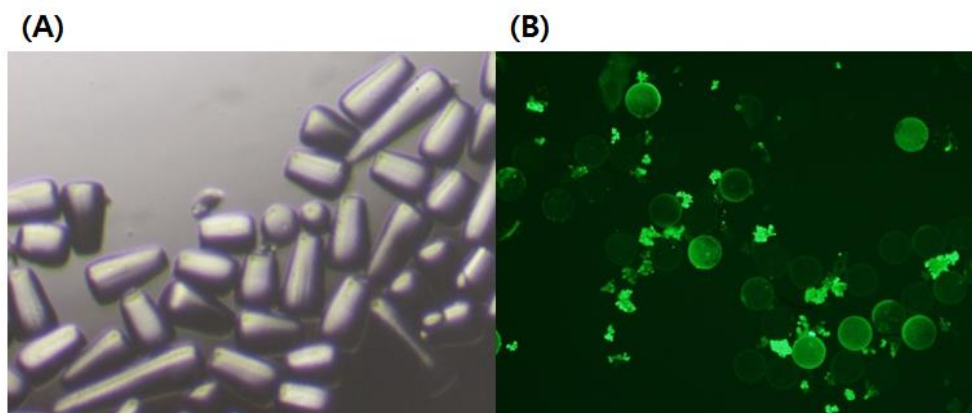


Figure 6. Problems in the bead during the mass production process.
(A) Variation of shape. (B) variation of signal.

However, while it was possible to publish papers through small scale production and selection as a proof of concept, there were many problems for real application of this technology in hospitals or diagnostic fields. First, absolute production volume was far too low. Most diagnostic kits have a shelf life of about one year. Assuming that 5,000 beads are used per well of 96-well plate to test one patient, and 100 patients are tested per day, about 180 million beads are needed per year. However, when I joined the lab, daily production capacity was under 100,000 beads. It means that three years were required to produce the beads to use for one year. Second, variation occurring during production process was very serious. The beads in figure 6A, it was intended to produce same beads but the result was terrible. It was due to try to mass fabrication in laboratory setup unsuitable for mass production. Figure 6B shows different signals even though they were produced in one reaction chamber. i.e., theoretically should show same signal. This means surface functionalize chemistry which allows biomarker

to bind on bead surface is unstable. Third, there was no software for decoding beads. In figure 5B, code of each bead were not recognized by software but determined by looking at it with naked eye. An automated analysis software is necessary for real application, and also development of effective code assignment method was required.

In this dissertation, the process of developing encoded bead-based multiplex assay technology from proof of concept to level that can be used in actual diagnosis is described. And then, clinical application in Alzheimer' s disease (AD) is described as an application among the various clinical application results.

Chapter 2. Platform development

In this chapter, the entire process for developing multiplex assay platform is described. These processes include magnetic nanoparticle synthesis, scaffold formation, Silica coating, surface functionalize, coupling, assay, and decoding program. The platform was developed under the supervision of Quantamatrix Inc. (Seoul, Republic of Korea), so it was named as quantamatrix multiplex assay platform (QMAP™).

2.1. Synthesis of superparamagnetic nanoparticle

To handle beads comfortably and to enable automation, it is necessary to give magnetism to the beads. During the process of surface treatment of beads or during the assay process, it is repeated the process of reacting and washing with various reagents. In this process, it is much easier and more efficient to remove the supernatant by holding the beads with a magnet than by removing the supernatant using centrifuge or filtering.

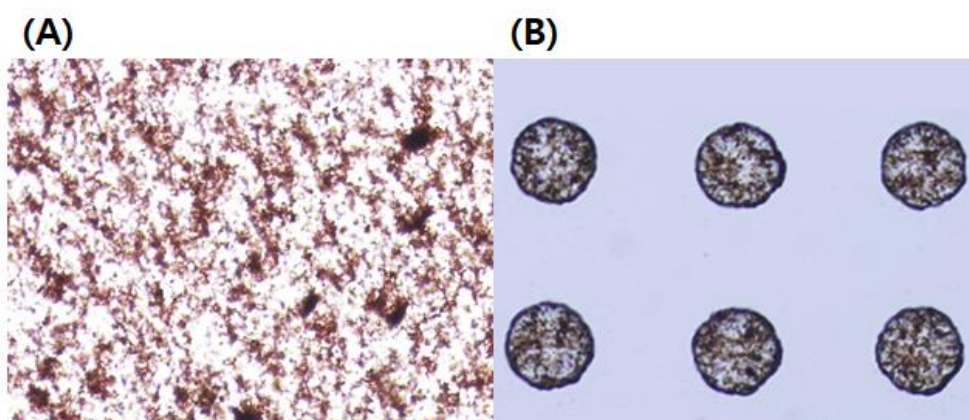


Figure 7. The result of mixing a typical magnetic nanoparticle in a polymer mixture. (A) Aggregation of magnetic nanoparticles in liquid polymer. (B) Incomplete polymerization of beads.

When commercially available magnetic nanoparticles were applied to polymer mixture, there is severe problem in precise photo-polymerization patterning due to their ferromagnetic properties (Figure 7). Magnetic nanoparticles mainly synthesized with Fe_3O_4 are not transparent and block or reflect the light. Ferromagnetic magnetic nanoparticles form large lumps through attraction with each other in liquid polymer. That is, magnetic nanoparticles do not distribute evenly but irregularly distribute in large lumps so when patterned UV is illuminated at polymer irregular reflection occurs and takes on irregular shape.

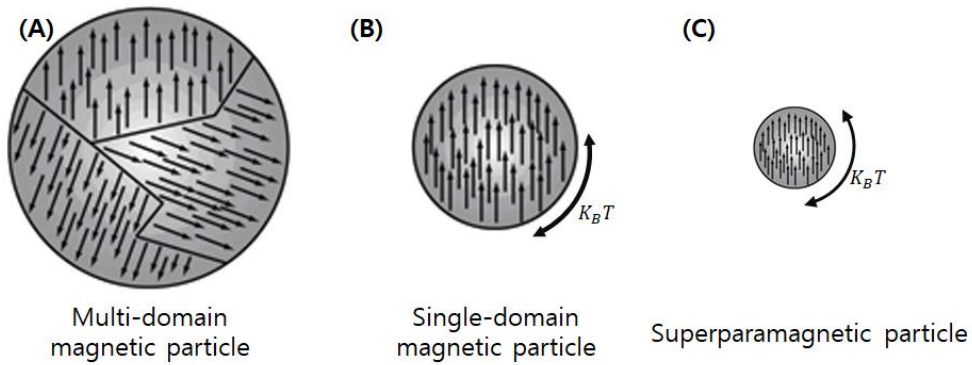


Figure 8. Differences in domains according to the size of magnetic particles. (A) Magnetic particles over 130 nm. (B) Magnetic particles between 130 nm and 20 nm. (C) Magnetic particles less than 20 nm [20]..

To avoid this problem, superparamagnetic magnetic nanoparticles must be used. Superparamagnetism means that it has magnetism when an external magnetic field is applied but loses magnetism when the external magnetic field disappears. The main factor that affects whether magnetic particles become ferromagnetic or superparamagnetic is the size of the domain which is the minimum unit when particles are formed (Figure 8) [20]. Large magnetic particles consist of multi-domain magnetism. When the size of a magnetic particle becomes smaller than 130 nm, the magnetic particle becomes single-domain magnetism. However, its magnetism is stronger than thermal disturbance, so once magnetism is formed by external magnetic field, it maintains magnetism even if external magnetic field disappears. When size of magnetic particle is reduced below 20 nm, thermal disturbance becomes stronger than magnetism and does not have magnetism in absence of external magnetic field. Such magnetic nanoparticles are called superparamagnetic nanoparticles.

However superparamagnetic nanoparticle has disadvantage that its magnetism is too weak. If excess amount of magnetic particles were mixed in polymer mixture to overcome weak magnetism, UV light cannot reach to the polymer layer and normal polymerization does not occur. To overcome weak magnetism, I introduced superparamagnetic colloidal nanocrystal clusters (CNCs) [21]. By making clusters in specific sizes and shapes, sufficient space for UV

light to pass through while using same amount of magnetic particles can be secured. Also, it's magnetism is increased due to distance between magnetic domains disappeared and act as multiple domain of large magnetic particles. By mixing such synthesized magnetic nanoparticles with polymer and performing UV patterning, the encoded beads which have sufficient magnetism can be made (Figure 9).

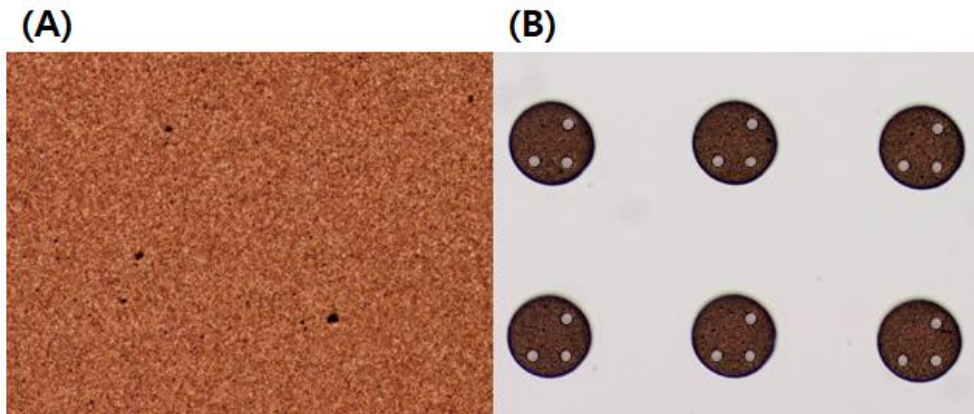


Figure 9. The result of mixing superparamagnetic nanoparticles into a polymer mixture. (A) Even the distribution of magnetic nanoparticles in the liquid polymer. (B) Bead shape and code are clearly polymerized.

2.2. Implementation of optical setup for mass production

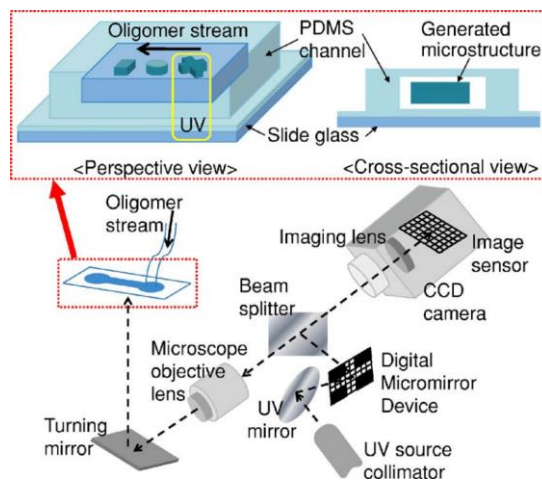


Figure 10. Schematic diagram of the proposed optofluidic maskless lithography system for dynamic control of the photopolymerization process in microfluidic devices [19].

Optofluidic maskless lithography (OFML) system is basic technology in my lab[19]. Figure 10 schematically describes the experimental setup, which combines a high speed optical projection system for dynamic UV photo-patterning, a microfluidic channel for UV-curable polymer stream, and a microscopic imaging system for inspection and monitoring. One advantage of using UV-curable polymer is that they can be readily fabricated into a variety of shapes by photo-polymerization; this characteristic is both powerful and versatile as it allows for nearly limitless coding capacity[22–27]. A high intensity mercury xeon lamp with a fiber based light guide is used as a continuous wave light source for photo-polymerization. A 10x microscope objective lens projects the computer controlled image pattern on the micro mirror array to the final object plane. The optical projection system and imaging optics share the same objective lens and their light paths are separated by a beam splitter. The microfluidic channel is located on the common object plane of the projection system and microscope. To monitor the polymerization process and the fabricated microstructures at the object plane, a microscopic imaging system with a charge coupled device image sensor was introduced. In this lithography setup, a high speed optical projection system with a two dimensional array of micro mirrors dynamically controls the UV exposure pattern, and makes it easy to fabricate a variety of microstructures in real time without having to prepare for photomasks.

UV-curable polymer consists of trimethylolpropane ethoxylate triacrylate (ETPTA) as the main scaffold of bead, 3-(trimethoxy silyl) propyl acrylate (TMSPA) as the seed of silica coating, DAROCUR 1173 which initiates photo-polymerization, and super paramagnetic nanoparticles which described above. The microfluidic channel for UV-curable polymer stream is made of polydimethyl siloxane (PDMS). The oxygen contents near the PDMS surface prevent the photo-polymerization process, and thus allow the formation of free-flowing polymeric microstructures inside the channel. Oxygen layer that prevents photo-polymerization on

PDMS surface is called oxygen inhibition layer [28].

Although OFML technology has advantage that shape of bead can be easily changed in real time, as described in introduction, there are limitations in producing enough volume to use for real diagnosis application. Although it takes only a few milliseconds to make one bead, interval time between pushing out produced bead through flow, waiting for polymer stream to be stabilized, and then illuminating UV again is long so number of beads that can be produced in one hour does not even reach to 1,000. Second, the amount of polymer is too much wasted when pushing bead with flow. TMSPA, one of the main component in UV-curable polymer mixture, has high unit price so waste of polymer causes severely increased the production cost. Third, when photo-polymerization is repeated at one location, oxygen layer on PDMS surface becomes depleted and bead sticks to PDMS channel.

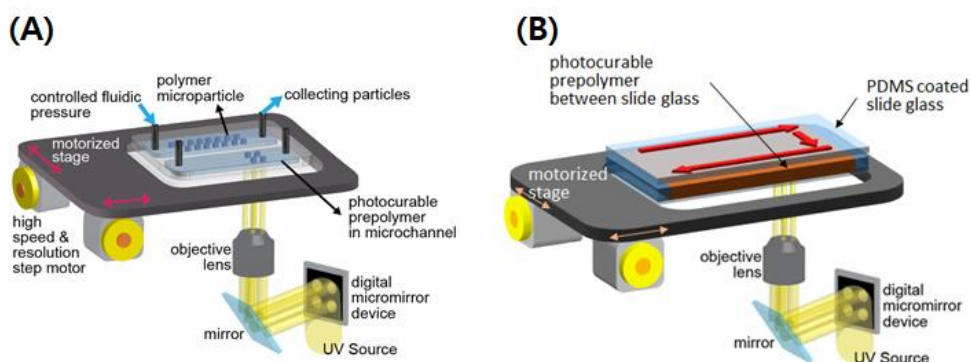


Figure 11. Intermediate systems developed for mass production. (A) Photo-polymerization occurs in the PDMS channel or (B) occurs between PDMS-coated glasses.

Figure 11 lists the setups I tried to increase bead productivity. The first method was to link a motorized stage to solve the problem of depletion of the oxygen inhibition layer by change the location where photo-polymerization was repeated (Figure 11A). However, although it was less frequent than previous setup, eventually the oxygen inhibition layer disappeared and the bead sticking problem occurred when photo-polymerization was performed for a long time. Also, the problems of poor productivity and waste of polymer was

still remained.

Even if photo-polymerization is performed at various locations in PDMS channel using motorized stage, channel area has limitations so it is inevitable to repeatedly polymerize at same location. To make polymerization is occurred only once at each location, a method using slide glasses which have larger area than microfluidic channel was devised (Figure 11B). Two slide glasses are coated with PDMS so that bead does not stick to slide glass, and UV-curable polymer is filled between two slide glasses. The height of polymer layer is adjusted by placing tape or film that can select thickness between two slide glasses as spacer. As a result, it is possible to completely solve problem of depletion of oxygen inhibition layer and waste of polymer. Also, the interval time between UV illumination can be reduced. However, unlike PDMS channel which the height can be uniformly controlled, there is a lot of variation in height while attaching the spacer by hand. So shape of bead was not uniform as shown in figure 6A. Also there is still fundamental limitation of production volume, i.e., interval time between forming one bead at a time, moving the stage, and then forming another bead again. With this setup, the maximum amount that can be produced in one hour is 20,000 beads. Although it is a 10 times improved result compared to the previous OFML setup, it was still far from enough to mass produce at the billion level.

Although OFML based system has advantage that desired shape of bead can be easily made by controlling UV pattern in real time, the method of producing one particle at a time has limitations in mass production. So I tried photolithography method used in semiconductor process which performed in large area. A single iteration of photolithography combines several steps in sequence: 1) spin coating photoresist (PR) on wafer, 2) prebaking to drive off excess photoresist solvent, 3) exposing patterned UV through photomask engraved with pattern, 4) post exposure baking (PEB) to reduce interference effect from other light after UV exposure, 5) developing to remove part exposed or not exposed to patterned UV, and 6) hard baking to completely harden shape. However, there was

critical problem in making polymer bead with conventional semiconductor process. In conventional semiconductor process, prebaking hardens liquid PR to solid so that PR does not stick to mask during next process UV exposure. However, UV-curable polymer lost its property of reacting with UV as soon as prebaking was done. If liquid polymer is used directly in semiconductor UV exposure without prebaking step, there is very high risk of equipment failure. For these reasons, it was necessary to develop UV exposure equipment customized for polymers other than PR. Many part of machine is similar to conventional UV exposure machine. The difference from the conventional machine is that the photomask is not attached to the equipment, but is assembled with photomask-polymer-slide glass and loaded onto the UV stage. An outlet is added to flow out the liquid polymer from the assembly of the photomask-polymer-slide glass to prevent the equipment failure.

UV-curable polymer shrinks when photo-polymerized by UV. This causes micro flow around bead but since only one bead is produced at a time in OFML setup, such flow has little effect on polymerization. Also since UV light is condensed through objective lens and increased intensity per unit area greatly in OFML system, so polymerization completes within few milliseconds and influence by flow also decreases (Figure 12A). On the other way, UV is spread widely to expose over wide area at same time in the large area UV exposure system, UV intensity per unit area decreases greatly compared to OFML (Figure 12B). Therefore, it takes more than 2 to 4 seconds for polymerization. It means that even if only the flow at the same level as the flow in OFML, it is more affected by flow. In addition, in a large area system, a much stronger flow occurs as the polymer shrinks simultaneously over a large area. As a result, beads produced in large area setup were severely deformed and precise code assignment was impossible (Figure 12C).

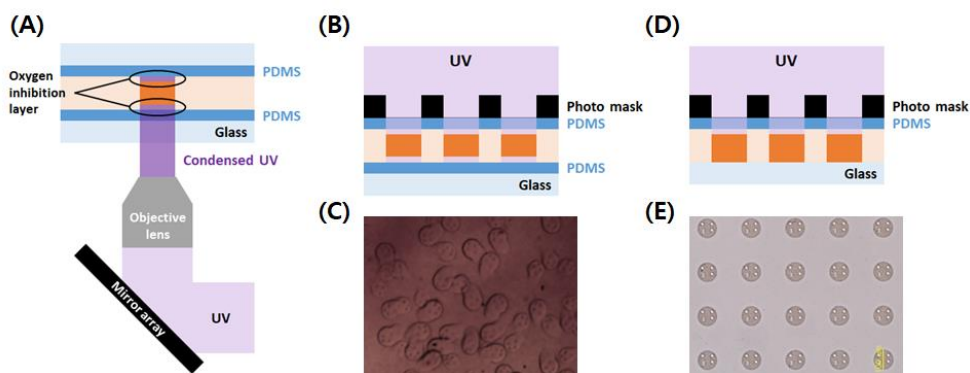


Figure 12. Cause and solution of deformation in large area UV exposure system. (A) Concept image of the OFML system. (B) Concept image of the large area system. (C) Deformed bead image. (D) Improved image of the large area system. (E) Deformation resolved result.

Several attempts to solve this problem were tried, but the solution was surprisingly simple. In OFML, oxygen inhibition layer of PDMS was actively used to push out beads formed by polymerization in order to repeat photo-polymerization at the same place. However, beads attached to glass substrate while polymerizing were easily separated from glass substrate by lightly scratching. The cause of the deformation in large area UV exposure setups is the floating and moving of beads caused by flow. Deformation problem can be solved by anchoring on the glass substrate without PDMS coating (Figure 12D and E).

The final production protocol is as follows: 1) coat PDMS on photomask where patterned shape of bead, 2) load UV-curable polymer onto photomask, 3) cover with slide glass with spacer attached so that UV-curable polymer spreads evenly between photomask and slide glass, 4) put the assembly of photomask-polymer-slide glass on UV exposure stage, 5) UV illumination, 6) separate photomask and slide glass and wash off non polymerized polymer with ethanol, 7) scrape the beads attached to the glass substrate with a scraper and collect them in the tube.

	OFML	Modified OFML	Large area
Glass/Channel	PDMS coating (5min) Channel attach (5min)	PDMS coating (5min)	SAM coating (3min)
Spacer/Polymer	–	1 min	4 min
UV exposure	< 100 ms for 1 bead	< 100 ms for 4 beads	2~4 sec for 880,000 beads
Interval between exposure	1~2 sec (flow stabilization)	< 1 sec (stage moving)	–
Number of exposures	< 1,000 times	About 10,000 times	1 time
Gathering	Real time	1 min	2 min
Cleaning	One time use only	1 min	4 min
Time required for one-round	–	2 hr	15 min
Production in one-round	< 1,000 beads	40,000 beads	880,000 beads
Production per hour	< 1,500 beads/hr	20,000 beads/hr	3,520,000 beads/hr

Table 1. Comparison of bead production in three setups.

In original OFML setup, one bead is made at a time in PDMS channel then bead is pushed out through flow then waits for flow to stabilize then repeats process of making another bead. It takes several seconds to push out bead through flow and wait for stabilization so number of beads that can be produced in one hour does not exceed 1,500 beads. In setup using two slide glasses coated with PDMS, the stabilization time at channel based OFML is greatly reduced and hourly bead production increases to about 20,000 beads. However, it is still far from enough to mass produce at billion level. In large area UV exposure setup about 880,000 beads are produced in 4 seconds. Overall time for pre-illumination and post-illumination takes about 15 minutes. As a result, hourly production increased to 3,520,000 beads which is 2,300 times more than original OFML setup and 176 times more than method combining two slide glasses and OFML.

2.3. Solving cracks of silica layer

Polymer beads have the advantage of being easily fabricated into any desired shape. However, bio-conjugation by photo-polymerization of acrylate modified biomolecules can be sensitive to the chemical environment, and such polymer-based beads are easily damaged by chemical and mechanical stimuli[29]. Furthermore, small molecules can be absorbed into the polymer matrix, thereby amplifying the detection error[30,31]. In previous study, a strategy for fabricating shape encoded bio-conjugatable silica-coated beads was suggested[18]. This method uses the complicated geometrical structure of the polymeric bead for identification, but takes advantage of the stable chemical and physical properties of silica[32,33]. When fabricate polymeric beads, a pre-polymer resin composed of the 10 : 1 volumetric ratio of ETPTA and TMSPA was prepared as a photo-curable material containing acrylate groups for the polymer scaffold. TMSPA serves as the silane-grafting material that participates in silica formation. Then, the polymer beads were coated with silica by a modified version of the Stober method[34,35]. This process allows for the direct and rapid application of silica coatings onto silicon-grafted beads via a single step.

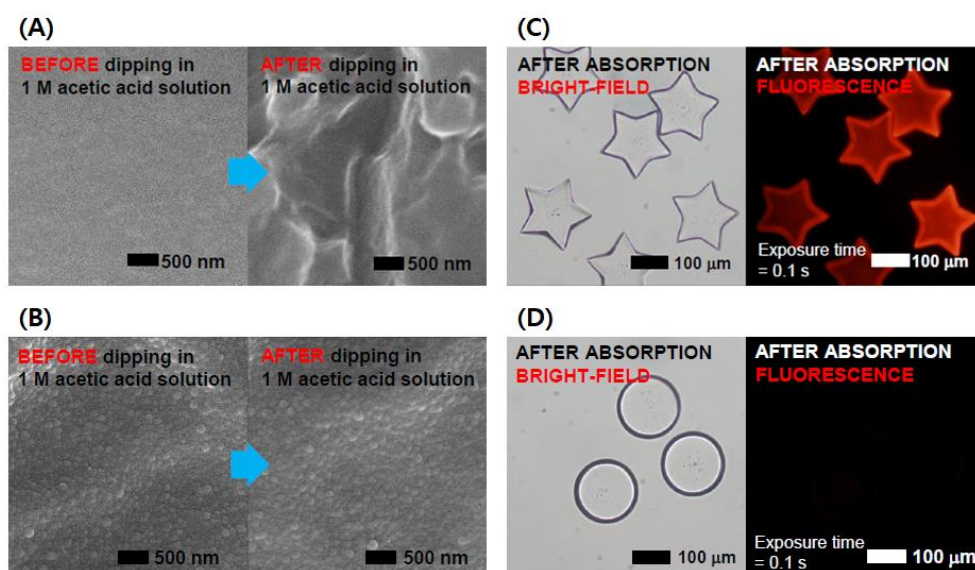


Figure 13. Effect of silica layer coating. (A) Surface damage of bead in

dipping to 1M acetic acid without silica coating and (B) with silica coating. (C) Nonspecific absorption of bead without silica coating and (D) with silica coating[18].

Figure 13 shows chemical stability and molecular absorption characteristics of polymer bead with- and without- silica. When beads are dipped in 1M acetic acid solution, bare polymer bead is damaged by chemical (Figure 13A) while silica coated bead remains stably preserved (Figure 13B). Chemical stability is important because high reactivity solvents such as dimethyl formamide (DMF) are used in the process of modifying the surface with amine and carboxylic acid. If silica coating is not done, polymeric beads dissolve completely in DMF and the beads disappear. Only when silica coating is done completely, the shape of the bead remains as it was initially designed. When using bead for bioassay fluorescent dye should only bind to probe in cascade form. However, since polymer beads have porosity, they absorb fluorescent dyes non-specifically (Figure 13C). In this case, even if a cascade reaction does not occur, non-specific absorption causes the bead to generate a signal, making it impossible to use in bioassays. Polymer beads can be used for bioassay only when a silica layer is coated to prevent non-specific absorption (Figure 13D).

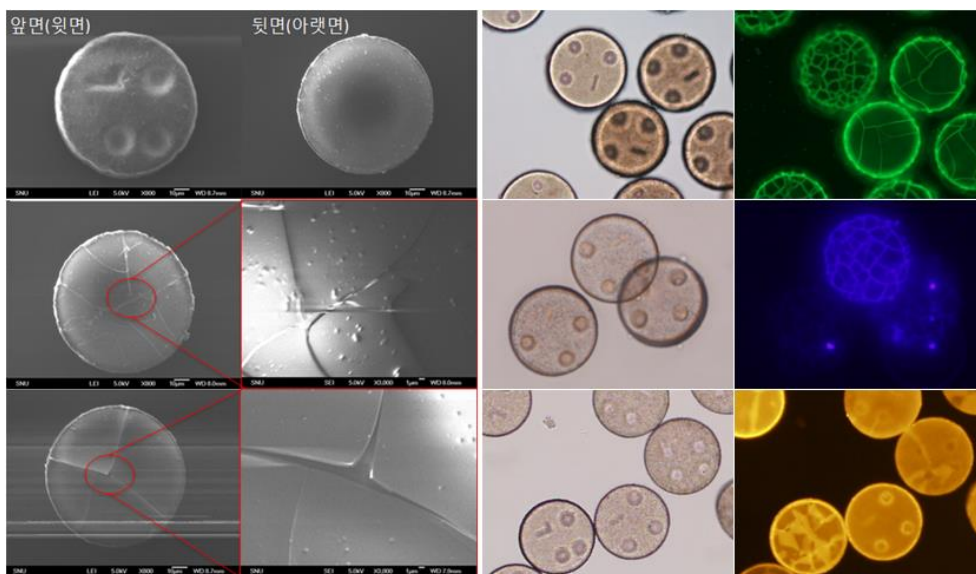


Figure 14. The cracks occurred with large area UV exposure system.

After producing beads with large area UV exposure system, frequency of crack occurrence after silica coating increased dramatically (Figure 14). I tested various factors such as type of polymer, molecular weight of polymer, ratio of polymers, concentration of magnetic nanoparticles, and silica coating recipe. The cause finally found was the use of bare slide glass without PDMS coating.

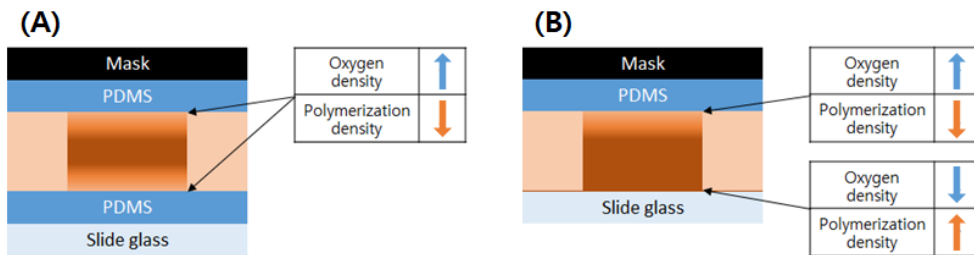


Figure 15. (A) Polymerization with PDMS coating on both sides. (B) Polymerization in the state where only one side is coated with PDMS.

Oxygen density is high near PDMS surface and decreases as it gets further away from PDMS surface. Oxygen interferes with photo-polymerization, and polymerization density also changes depending on oxygen concentration. In OFML system, beads were fabricated in PDMS channel or between PDMS coated slide glass, so polymerization densities between front and back side of bead were same (Figure 15A). In large area UV exposure system, only one side was coated with PDMS while opposite side slide glass was not coated with PDMS, so polymerization densities between front and back side of bead were differed (Figure 15B). As a result, bending occurs due to difference in density between two sides of bead resulting in crack in silica layer. To verify the hypothesis, I fabricated beads under conditions where both sides were coated with PDMS or only one side was coated with PDMS, respectively, in OFML system and large area UV exposure system, and were able to prove hypothesis (Figure 16).

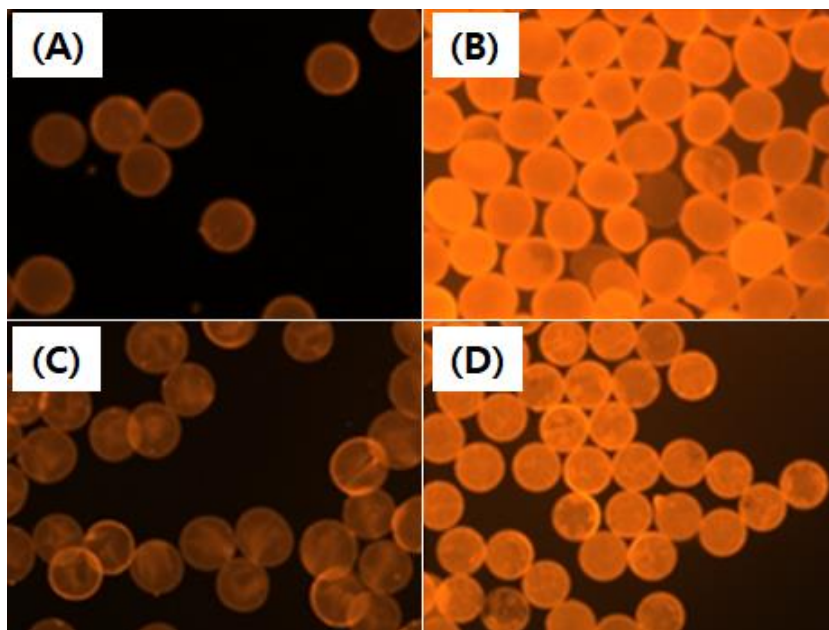


Figure 16. Differences in bead shapes and silica cracks generated under various conditions. (A) Bead is polymerized between PDMS–PDMS in OFML system. (B) Bead is polymerized between PDMS–PDMS in large area system. (C) Bead is polymerized between PDMS–Glass in OFML system. (D) Bead is polymerized between PDMS–Glass in large area system.

To resolve density difference between two sides of bead, either both sides must be coated with PDMS or neither side must be coated with PDMS. If both sides are coated with PDMS, problem of deformation of bead occurs again. So I devised method not using PDMS. Since polymer is close to hydrophilic, I coated photomask surface with self-assembled monolayer (SAM) having hydrophobic properties instead of using oxygen's interference effect on polymerization to prevent bead from sticking to photomask. However, probability that bead sticks to photomask increases compared to physically not touching photomask with PDMS coating. Of course, such attached beads can be detached without exerting great force but damage to photomask which is expensive and must be used repeatedly had to be avoided at all costs. To reduce probability that bead sticks to photomask, plasma treatment was applied on opposite side slide glass to make it more hydrophilic. However, if plasma treatment is excessive and hydrophilicity

becomes too strong, damage may occur on bead during process of detaching it, so it was necessary to establish appropriate plasma treatment protocol.

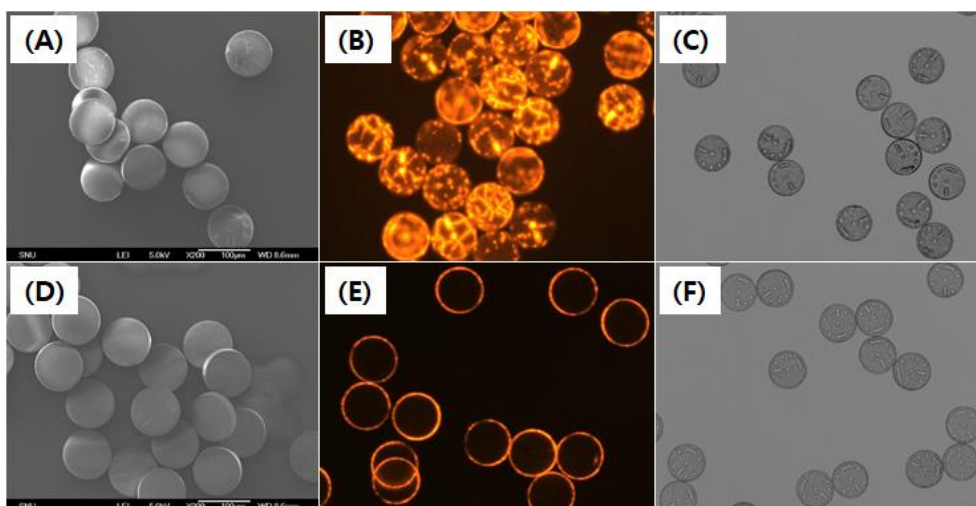


Figure 17. The difference in crack and resolution before and after improvement. (A) SEM, (B) fluorescence absorption, and (C) bright field images of the beads produced in PDMS-bare Glass. (D) SEM, (E) fluorescence absorption, and (F) bright field images of the beads produced in SEM-plasma Glass.

Through the modified protocol, cracks in the silica layer were completely resolved (Figure 17). Secondly, as the physical thickness of the PDMS layer of about 50um disappeared, the distance between the photo-mask and the UV-curable polymer was reduced, resulting in improved resolution (Figure 17C and F).

2.4. Functionalize the surface of the bead

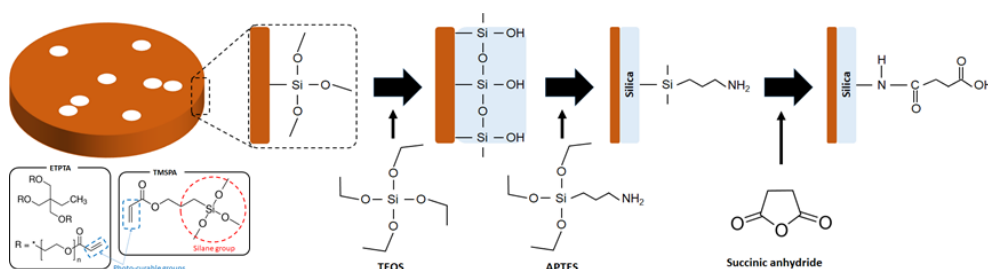


Figure 18. Overall process of surface functionalization.

Figure 18 shows the process of chemical modification of bead surface. UV-curable polymer consists of ETPTA which is main material of scaffold and TMSPA which becomes seed when silica coating. After scaffold formation, silane seed of the bead reacts with tetraethylorthosilicate (TEOS) to form silica layer on bead surface. (3-Aminopropyl) triethoxysilane (APTES) is bonded on top to change bead surface from silica to amine, and then reacts with succinic anhydride to make carboxylic acid on the bead. Later, when using bead for bioassay, carboxylic acid on bead surface couples with amine of amine modified DNA or protein [18].

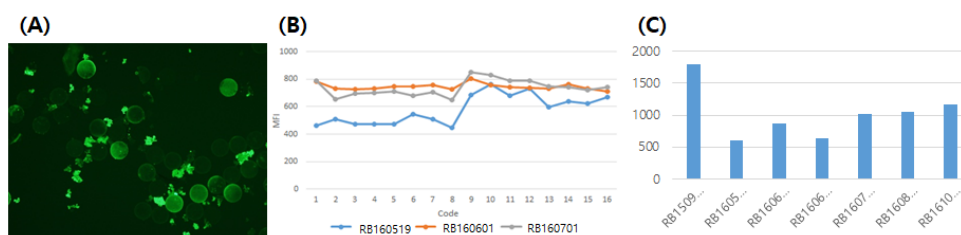


Figure 19. (A) Variation within a reaction chamber. (B) Variation between codes. (C) Variation between lots.

However, beads produced by above protocol were quite unstable. Even between beads produced in one reaction chamber, the signals were different. Also, signals were different between codes that should have same signal by coupling same probe and lot variation was also very serious (Figure 19).

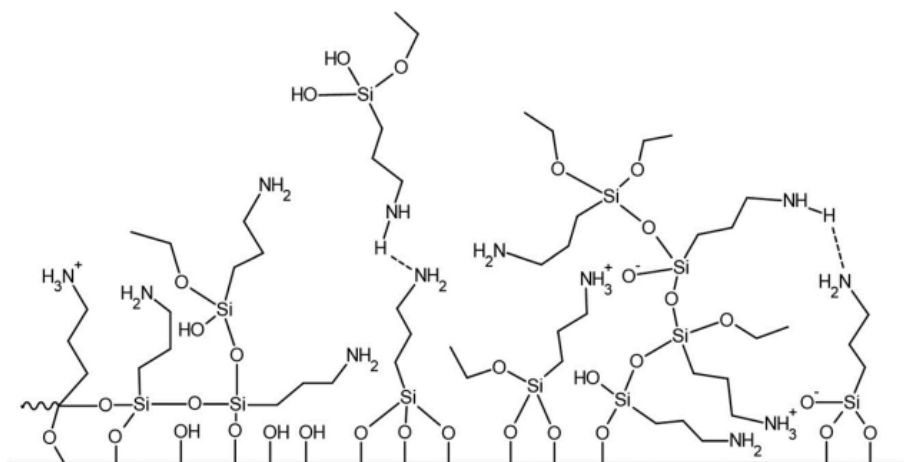


Figure 20. Schematic representation of aminosilane self-polymerization occurring on the diatomaceous earth silica surface [36].

The first cause of this variation problem is that APTES is coated on bead through silanization process through complex reactions such as covalent bonding, hydrogen bonding, electrostatic attraction, horizontal polymerization, vertical polymerization, and interaction with functionalities present at interface. As a result, APTES layer form multilayer randomly rather than single layer (Figure 20) [36]. Especially this process is greatly influenced by moisture absorbed by reagent and moisture in workspace, and it is very difficult to control precisely [37,38].

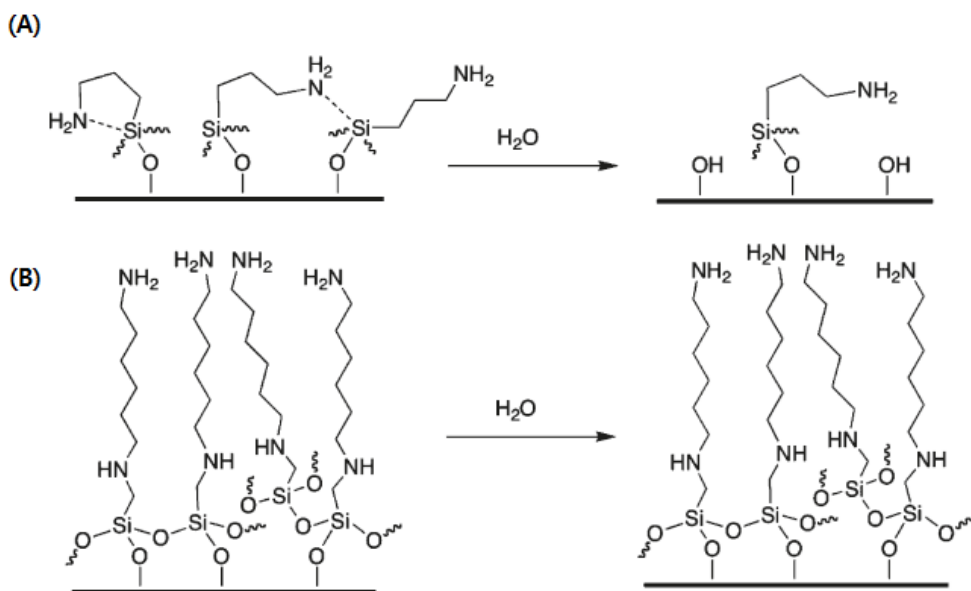


Figure 21. Hydrolysis reaction in (A) APTES and (B) AHAMTES[39].

The second cause of variation is that amine of APTES itself acts as nucleophilic catalysts in hydrolysis[40–42]. The final process of bead production and bioassay process takes place in solvent based on water. APTES layer on bead is easily hydrolyzed due to nucleophilic catalytic reaction of amine. Even, the last remaining APTES on bare silica layer disappears through intra-molecular hydrolysis by forming 5-ring itself or inter-molecular hydrolysis by decomposing surrounding APTES (Figure 21A) [39].

I found a material called N-(6-aminohexyl) aminomethyl triethoxysilane (AHAMTES) as a substitute[39,42]. AHAMTES also forms multilayer through various and random reactions like

APTES. In this case, direction in which amine binds can be sideways or upside down, and amine acts as nucleophilic catalysts to hydrolyze silane like APTES. However, difference between AHAMTES and APTES reveals when last single layer remains. AHAMTES has long carbon chain so it does not undergo intra-molecular hydrolysis by making ring by itself. For same reason, amine cannot touch silane at center of surrounding AHAMTES so inter-molecular hydrolysis also does not occur (Figure 21B). Table 2 shows change in thickness due to hydrolysis in both APTES and AHAMTES. Known size of single APTES molecule is 10 Å. In case of APTES almost all APTES layers disappear after being exposed to water for 24 hours. In contrast, silane layer of AHAMTES is remained as single layer.

(A)				(B)			
Silanization time (hr)	Initial (Å)	After 24h (Å)	After 48h (Å)	Silanization time (hr)	Initial (Å)	After 24h (Å)	After 48h (Å)
1	4	< 1	< 1	1	11	9	10
1.5	4	< 1	< 1	2	14	10	10
3	10	1	1	4	22	9	10
19	57	2	1	8	27	9	13
				16	30	11	12

Table 2. Thickness of silane layer as a function of silanization time and after exposure to water. (A) APTES-derived silane layer. (B) AHAMTES-derived silane layer [42].

I changed main reagent based on this paper, and revise overall reaction conditions such as buffer, catalyst, temperature, time, etc. The silanization reaction is very sensitive to the environment condition, especially humidity, and this was also the case for AHAMTES. To control the process environment, the process was performed in a clean room where temperature and humidity were controlled. However, even in the clean room, the humidity was not 0%, so it was impossible to perfectly control the silanization reaction. Instead, a strategy was devised to remove the silane layer by intentional hydrolysis after reacting AHAMTES in multi-layers by excessive silanization. What made this possible is the use of the characteristic that the last silane layer derived from AHAMTES is not decomposed by hydrolysis, while the silane layer derived from

APTES completely disappears by hydrolysis. Through this method, it is possible to maintain a constant amine content on the bead surface and reduce variation in functional groups by applying carboxylic acid on top of the controlled amine. Carboxylic acid making condition is also revised greatly due to large change in amine content compared to previous protocol.

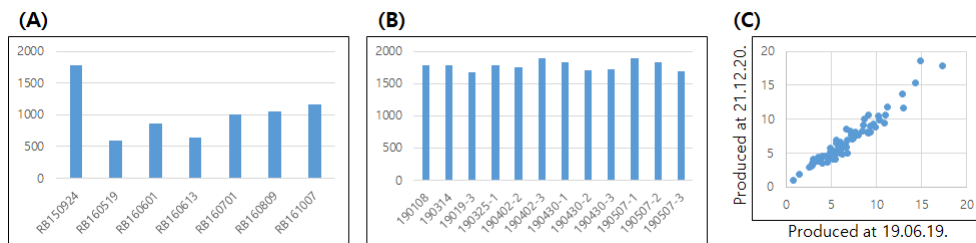


Figure 22. (A) Lot variation before improve of surface functionalization (CV 36.2%). (B) Lot variation after before improve of surface functionalization (CV 3.9%). (C) Correlation between the beads produced in June '19 and December '21 (correlation coefficient 0.964).

Beads produced with changed protocol show quite stable signal. Previously, lot variation was very serious with coefficient of variation (CV) 36%. In contrast, lot variation over four months showed stable result with 3.9% in improved protocol (Figure 22A and B). After stabilizing functionalization of bead surface, Alzheimer' s disease diagnosis project started in June 2019 and clinical samples were stored in deep freezer. When the same sample was measured with beads produced in December 2021, the correlation coefficient with the previous result shows a very high result of 0.962 (Figure 22C). That is, even though there was an interval of 2.5 years, stability of production protocol was very excellent.

2.5. Development of coding scheme and decoding program

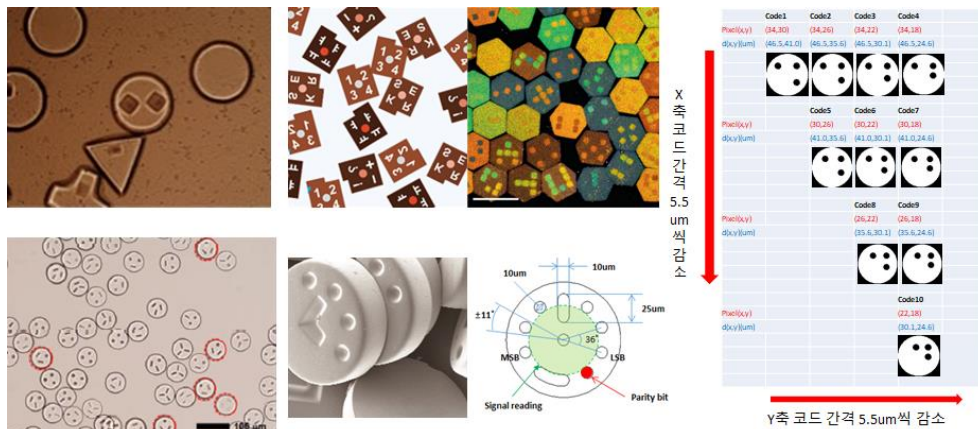


Figure 23. Coding schemes developed in BiNEL.

Polymer beads have advantage of being easily fabricated into any desired shape. Figure 23 includes coding methods devised in my lab and there are no limits to various ways codes can be assigned besides this. The circle shape was selected for physical stability because it is needed to use large amount of beads without damage for several years or more. The code based on shape can be misrecognized by poor scaffold making process, physical damage in storage, and incomplete focus during imaging. So, it is necessary to devise the way to prevent such misrecognition.

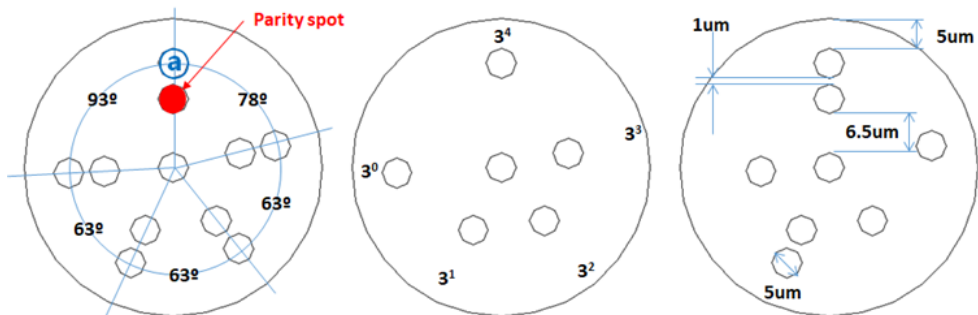


Figure 24. Encoding scheme developed for QMAP™.

Figure 24 shows the coding method currently used in QMAP™. This coding scheme has several advantages over existing methods. First, each hole must exist in at least one of 5 directions, and if for any reason a hole does not exist in one direction due to incomplete exposure, physical damage, imaging problems, etc., it is excluded

from recognition. That is, it acts as a first step misrecognition filter. Second, in previous coding methods, additional fiducial marks were placed to distinguish front and back of bead. On the other side, in developed coding scheme, angles between holes were differently assigned to distinguish front and back of bead. That is, by saving area sacrificed for fiducial mark, number of codes that can be assigned per unit area could be increased. Third, by adopting ternary system where hole exists only inside only outside or both in each direction, coding efficiency could be increased. Since there is no need to increase multiplicity than now, only 2 holes are placed in each direction. If higher multiplicity is required, 7-digit code can be implemented by placing 3 holes in each direction. Finally, by assigning one hole as parity spot like parity bit used to reduce error in electrical signal processing, possibility of misrecognition could be further reduced. With this implemented coding scheme, 122plex was implemented, and analysis program to be described next showed performance of 95% recognition rate and 0.5% misrecognition rate.

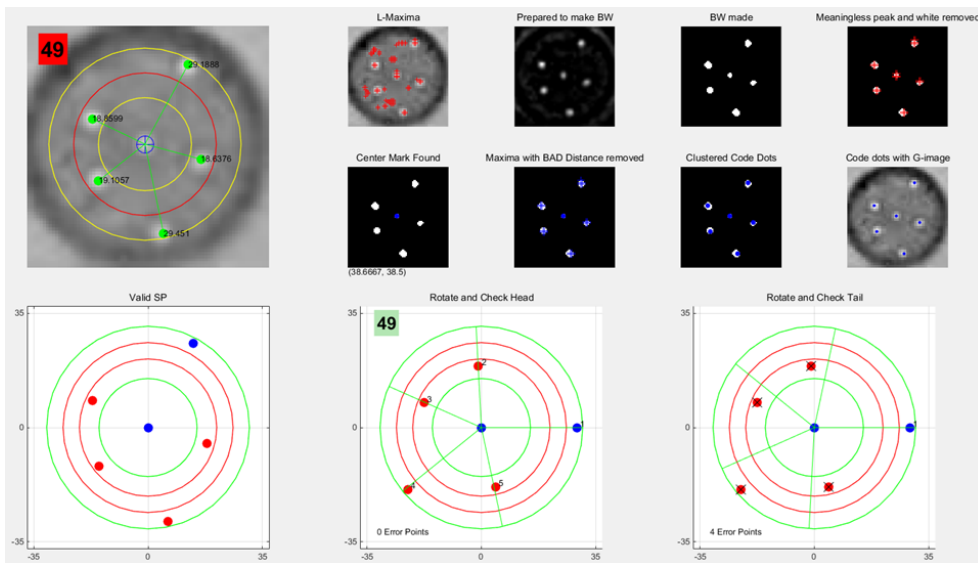


Figure 25. Image processing flow for decoding bead.

Figure 25 shows decoding process implemented using MatLab: 1) find beads through Canny edge detection, and cut out image [43], 2) enhance image contrast through sharpness enhance filter, 3)

search for local maxima and 4) create black and white (BW) image in parallel, 5) allocate the points overlapping between local maxima and BW image as hole (if multiple local maxima exist within one BW island, calculate average position of each local maxima and allocate as a hole), 6) calculate all angles between holes, 7) find reference hole commonly included in both 93° and 78° , 8) match with angle filter assuming both front- and back- side of bead is imaged to determine front and back of bead, 9) recognize position and number of holes in each direction and report final code number.

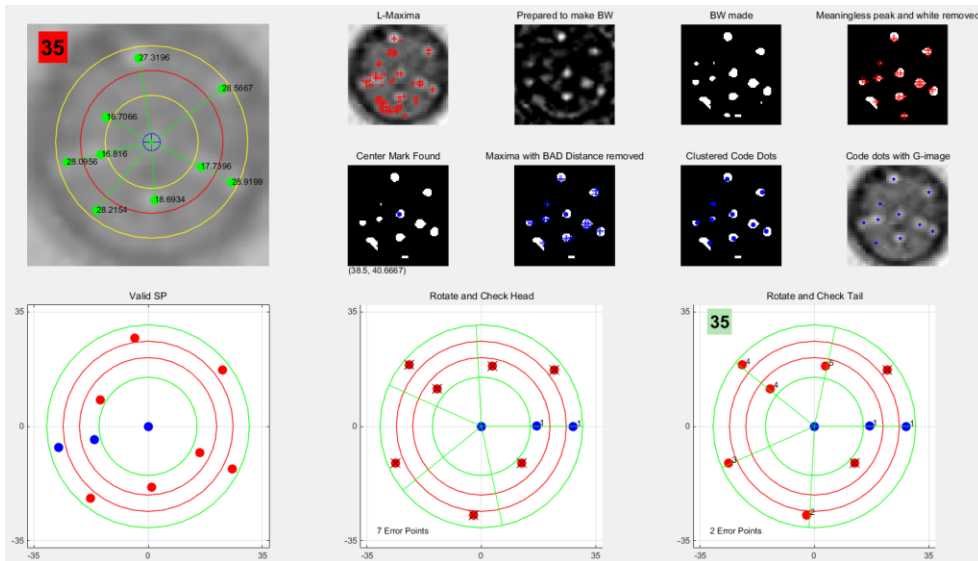


Figure 26. Image processing result of blurred image.

Figure 26 shows decoding process when focus is incorrect and hole is not clearly photographed. Even though local maxima and BW image are quite messy, decoding process reports the code number perfectly. Through this, it can be seen that developed encoding scheme and decoding software are quite robust.

2.6. Overall procedure to use QMAP™

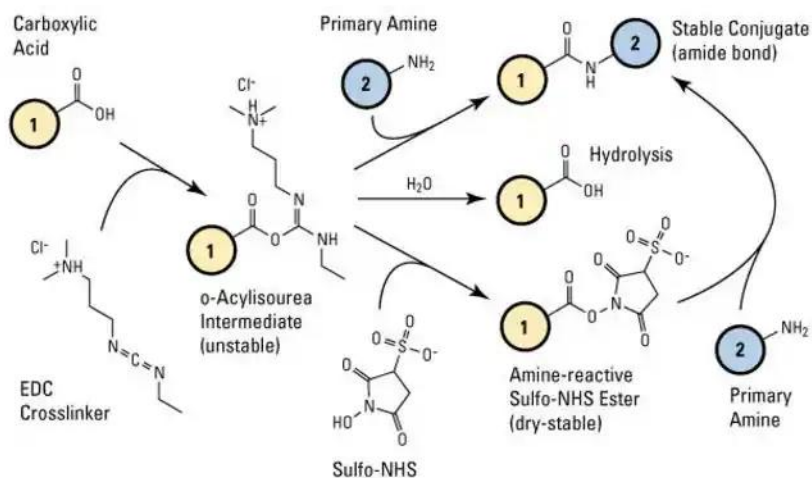


Figure 27. Coupling procedure between carboxylated bead and amine possess probe [44].

Carboxylated bead can be coupled with 5' -amine modified DNA or protein. Carboxylic acid on bead surface reacts with (1-ethyl-3-(3-dimethylaminopropyl) carbodiimide hydrochloride) (EDC) and N-hydroxysuccinimide (NHS) in turn to become activated state that easily reacts with amine. When coupling protein probe, carboxylated bead is activated with EDC/NHS, washed out EDC/NHS, and then reacted with protein probe. Protein has both amine and carboxylic acid itself. If protein is injected while EDC/NHS exists, EDC/NHS activates not only carboxylic acid on bead but also carboxylic acid on protein. In this case, amine on protein not only attaches to carboxylic acid on bead but also attaches to carboxylic acid on protein, i.e., reaction between proteins also occurs and reducing coupling efficiency. On the other hand, DNA does not have carboxylic acid. When coupling DNA probe, carboxylated bead, EDC/NHS, and amine-modified DNA are reacted together.

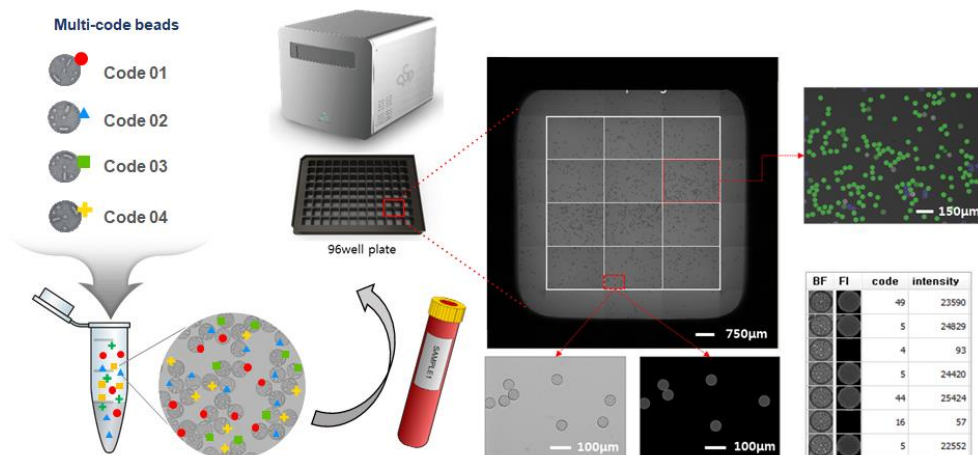


Figure 28. Overall procedure to use QMAP™.

The protocol for using QMAP™ is as follows. Mix probe coupled beads into one tube, and dispense into each well of 96-well plate. Inject different samples into each well. If biomarker exists in sample, the biomarker reacts with bead which matching probe is coupled. Wash out sample and inject detection fluorescent dye, usually streptavidin R-phycoerythrin (SAPE), then fluorescence appears from bead that reacted with biomarker earlier. Load 96-well plate into dedicated analyzer. The analyzer is combination of fluorescent microscope and motorized stage. Motorized stage searches location where beads exist and takes image with auto-focusing. After completing search for beads and focusing bright field image and fluorescence image are taken respectively from each field of view (FOV). Since size of bead is 50um and size of hole used for code assignment is 5um, imaging is performed with 10x objective lens. In this case, FOV becomes 1.80 x 1.35mm. 12 shots per well is taken for general 96-well plate and 6 shots per well is taken for QMAP™ dedicated 96-well plate.

In analysis software, code number of bead, i.e., type of biomarker is determined by decoding algorithm from bright field image. The amount of biomarker is measured with the brightness of each bead from the fluorescence image. During fluorescence imaging process, if some bead emitting very high signal, the signal of adjacent bead can be measured higher than original signal. To

reduce error from adjacent bead, only signal within 40% of radius is considered. If wash is incomplete during assay process, background noise may occur from well plate bottom. To compensate for this, histogram is drawn by collecting signals of all pixels in one image and values below signal with highest frequency are removed as background compensation. Type of biomarker recognized from bright field image and the amount of biomarker calculated from fluorescence field image are matched. To ensure reliability of results, 20~100 beads are used for each code. The beads that show upper- and lower- 10% signal are excluded as outliers. Through above process, final concentration of each biomarker in each sample is reported.

2.7. Efficiency comparison between ELISA and QMAP™

In the introduction chapter, the theoretical efficiency difference between ELISA and multiplex assay platforms is described. In this chapter, the real efficiency difference by comparing the specific protocols of ELISA and QMAP™ is described. The ELISA protocol was performed based on Bio-Rad' s sandwich ELISA with direct detection [45].

	ELISA	QMAP™
Coupling point	A day before the assay	Massive coupling and use for 1 year
Preparation	–	2 times wash EDC/NHS activation 1 time wash
Coupling	100 uL of capture antibody Concentration: 1~10 ug/mL (↔ 100~1000 ng/test) Overnight at 4 °C	15~50 ug of capture antibody for 400,000 beads (↔ 3.8~12.5 ng/test) Overnight at 4 °C
Washing	3 times wash	2 times wash
Blocking	150 uL of blocking solution 60 minutes at 37 °C	500 uL of blocking solution 60 minutes at 37 °C
Washing	4 times wash	1 times wash
Number of pipetting	9 times per 1 test	9 times per 4,000 tests

Table 3. Comparison of coupling protocol between ELISA and QMAP™ [45].

In ELISA, it is required the capture antibody to be coupled to a 96-well plate one day prior to assay. In contrast, the capture antibodies can be pre-coupled to beads corresponding to at least 4,000 tests and used for up to one year in QMAP™. Of course, in ELISA, capture antibodies can also be pre-coupled to a 96-well plate and used for a long period of time. However, in order to use pre-coupled antibodies for a long period of time, they must be stored in a refrigerator or freezer. Storing large volumes of 96-well plates in a refrigerator requires a large expenditure. In contrast, it is much easier to store beads for 4,000 tests in a 1.5ml tube in QMAP™.

There is also a significant efficiency difference in the amount of capture antibody required per test. In ELISA, 100~1000 ng of capture antibody is required per test, while in QMAP™ only 3.8~12.5 ng of capture antibody is required per test. In ELISA, coupling should be done individually for each well, so 9 times pipetting are required per test. In contrast, the same 9 times pipetting can be used to couple beads for 4,000 tests in QMAP™.

	ELISA	QMAP™
Sample reaction	100 uL of sample 90 minutes at 37°C	35 uL of sample 35 uL of detection antibody 30~90 minutes at 25°C
Washing	3 times wash	
Detection antibody reaction	100 uL of detection antibody 60 minutes at 37°C	
Washing	3 times wash	2 times wash
Fluorescence	100 uL of substrate solution 5~30 minutes at 25°C	50 uL of SAPE 10 minutes at 25°C
Washing	(Optional: add 50 uL of stop solution)	2 times wash
Number of pipetting	9 times per 1 sample	7 times per 1 sample
TAT	(coupling time) + 190 minutes	110 minutes

Table 4. Comparison of assay protocols of ELISA and QMAP™ when measuring one biomarker [45].

Even when using QMAP™ as a single plex assay, it shows higher efficiency than ELISA. 100 ul of sample is required per test in ELISA, while only 35 ul is required in QMAP™, a difference of

about 3 times. Similarly, detection antibody also requires 100 ul in ELISA but only 35 ul in QMAP™. In ELISA, the capture antibody is fixed to the bottom and the reactivity between probe and analyte is limited. In contrast, the QMAP™ beads coupled with capture antibody are suspended and the reactivity with analyte is much higher allowing for step simplification. The number of pipetting required is 9 and 7 respectively for ELISA and QMAP™ which does not seem like a big difference. However, this comparison is when using QMAP™ as a single plex.

	ELISA	QMAP™
Sample reaction	1,000 uL of sample 90 minutes at 37°C	35 uL of sample 35 uL of detection antibody (10x concentration antibody) 30~90 minutes at 25°C
Washing	30 times wash	
Detection antibody reaction	1,000 uL of detection antibody 60 minutes at 37°C	
Washing	30 times wash	2 times wash
Fluorescence	1,000 uL of substrate solution 5~30 minutes at 25°C	50 uL of SAPE 10 minutes at 25°C
Washing	(Optional: add 500 uL of stop solution)	2 times wash
Number of pipetting	90 times per 1 sample	7 times per 1 sample
TAT	(coupling time) + 230 minutes	110 minutes

Table 5. Comparison of assay protocols of ELISA and QMAP™ when measuring ten biomarkers [45].

In the case of multiplex assays, the efficiency difference between ELISA and QMAP™ widens. For example, when analyzing 10 biomarkers, ELISA requires 90 times pipetting to analyze one sample, but QMAP™ can still perform the assay with only 7 times pipetting. Another advantage of QMAP™ is that it greatly reduces the amount of sample used. For example, when analyzing 10 biomarkers, ELISA requires 1,000 uL of sample, but QMAP™ still only requires 35 uL. This is possible because multiple biomarkers in a sample react only with specific probes coated on beads. Therefore, even if the concentration of any biomarker changes due to its reaction with beads, it does not affect the reaction of other biomarkers with other beads. However, in QMAP™, additional tests

are required to check for cross-reactions between antibodies during kit development. This requires additional resources but considering the overwhelming efficiency of QMAP™, the benefits are much greater.

The turn-around time is also nearly twice as different when considering only the assay time: ELISA takes about 180 minutes and QMAP™ takes about 100 minutes. In ELISA, there is a limit to reaction efficiency because only the bottom of the well plate is coated with capture antibody. In contrast, in QMAP™, beads coated with capture antibody move actively while suspended and have higher reaction efficiency than in ELISA. Considering that capture antibodies must be pre-coated in ELISA a day before, the turn-around time difference more widens.

Chapter 3. Clinical applications in Alzheimer' s disease (AD)

Through the development of the bead mass production system, stabilization of surface functionalization, and development of the encoding scheme and decoding program, the platform, which had been a proof of concept, became available for real clinical applications. QMAP™ was applied to various clinical applications such as HPV[46], tuberculosis[47,48], sepsis[49], and AD[50–52] and showed excellent clinical performance. In this chapter, the results used for the clinical diagnosis of AD are described.

3.1. Advantages of blood-based diagnosis in AD

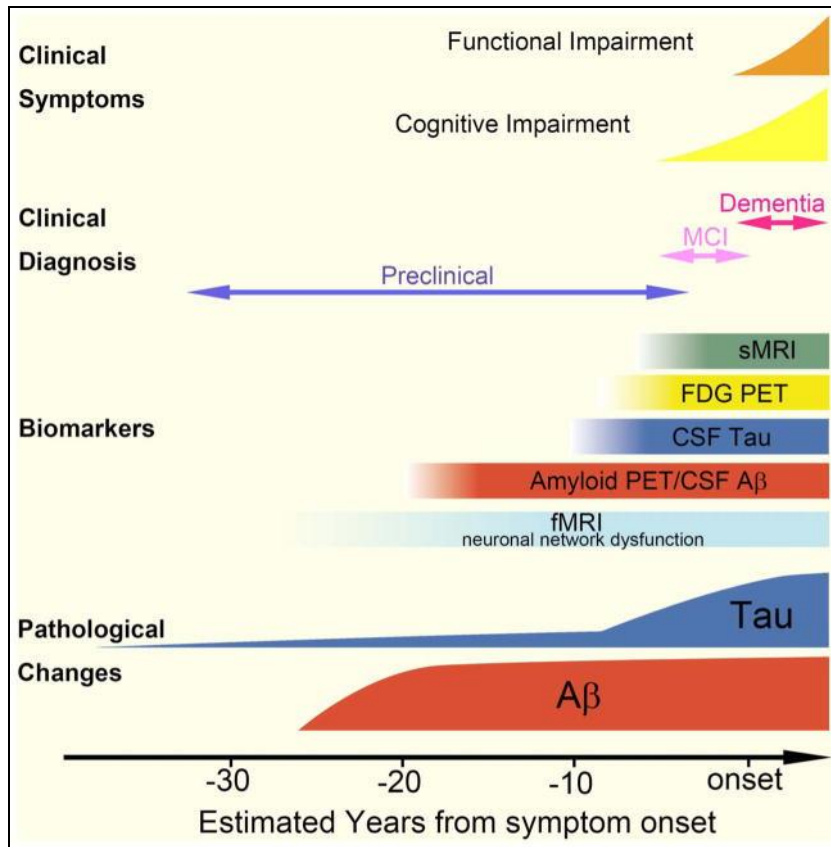


Figure 29. Chronological relationships among pathology, clinical symptoms and biomarkers[53].

AD is a neurological disease accompanied by the pathological features of beta-amyloid ($A\beta$) plaques and neurofibrillary tangles. AD is the most prevalent dementia and has a much earlier pathological progress than the onset of clinical symptoms (Figure 29) [53]; thus, many research efforts have sought to discover bio-fluidic biomarkers in the blood or CSF that can be used for early detection of the disease. Dementia cannot be cured or improved, but the progression of dementia can be significantly slowed.

Although direct brain-imaging methods using $A\beta$ -specific positron emission tomography (PET) ligands have been developed[54], PET is not an easily accessible method because of its high cost and radiation exposure. Especially in the early stages

of the disease, when pathological hallmarks exist in the brain but no clinical symptom is seen, patients would be unlikely to undergo a brain PET scan[55]. This a major obstacle when early diagnosis relies on PET. Many researchers and clinicians have noted that the use of efficient, early, and easily accessible diagnostic methods could prevent or delay the progress of AD pathology.

The other method to diagnose AD is neuropsychological assessment of dementia[56]. Cognitive abilities such as memory, frontal lobe and executive function, language and related functions, spatial and temporal composition function, and attention are measured over 2–3 hours. However, elderly people have a problem with such a long time-consuming questionnaire and intentionally give incorrect answers in order to receive treatment. Another method is to measure biomarkers in CSF. This method is clearly effective but extracting CSF causes considerable pain and burden to patients, so it is difficult to consider sampling CSF for routine health checkup and it is not suitable for early diagnosis.

Blood-based AD diagnosis has many advantages over the three diagnostic methods described above. It does not take long time for neuropsychological test and can exclude intentional bias during survey process. Compared to CSF, blood sampling is significantly less painful for patients. Since the multiplex platform can be diagnosed with a small volume sample, there is no need to collect additional blood for the test if it is introduced for health checkup. Although accuracy is lower than brain PET scans, the value as a screening tool is sufficient due to the cost is 10 times lower than PET imaging. Blood-based biomarkers for AD theoretically should enable early-stage disease detection or screening while also offering increased accessibility greater convenience and reduced cost[57].

However, there is a reason why blood-based AD diagnosis has not yet taken hold in the market. One reason for this is that only a small proportion of brain proteins are found in the blood, making it difficult to detect AD biomarkers. Additionally, the presence of high levels of plasma proteins, such as albumin and immunoglobulin G (Ig

G), in blood samples can cause analytical interference when measuring AD biomarkers[58]. The release of brain proteins into the blood stream may also cause degradation by proteases, leading to metabolization by the liver or elimination by the kidneys, and dilution thereof. This introduces variability that is not linked to changes in the brain and is difficult to regulate, thereby limiting the potential for discovering blood biomarkers of AD[59].

3.2. Development of QPLEX™ Alz plus assay kit

In a previous study, *Park et al* revealed a novel blood-based biomarker panel for cerebral amyloid deposition consisting of galectin-3 binding protein (LGALS3BP), A β 40, angiotensin-converting enzyme (ACE), and periostin (POSTN) [60,61]. When assessed by logistic regression analysis and receiver operating characteristic (ROC) curve analysis, these biomarkers combination exhibited a high area under the curve (AUC) and good sensitivity and specificity when blood levels were quantified through commercialized ELISA kits. For clinical practice and large population screening, they want a readily accessible diagnostic kit capable of measuring these biomarkers at once could critically enable the quick prediction of cerebral amyloid deposition.

The diagnostic efficacy and accuracy of the kit were evaluated for 300 cognitively diverse individuals who underwent Pittsburgh compound B (PiB) PET scans[51]. They consisted of 149 cognitively normal individuals (CN), 87 patients with amnesic mild cognitive impairment (MCI), and 64 patients with clinically diagnosed AD group. These individuals were recruited as part of the Korean Brain Aging Study for the Early diagnosis and prediction of Alzheimer's disease (KBASE). For QMAP™ assay, whole-blood samples were gathered in K2 EDTA tubes (BD Vacutainer Systems, Plymouth, UK) and centrifuged at 700 g for 5 min at room temperature. The supernatants were collected, and the tubes were stored at -80 °C. QMAP™ assay is performed as described in

chapter 2.6. Four beads encoded with different codes are fabricated and A β 40, LGALS3BP, ACE, and POSTN are pre-coupled respectively. QMAP™ assay is performed three times for 300 samples. All statistical analyses were performed using the Medcalc 17.2 software (Ostend, Belgium). To calculate the discriminatory power, sensitivity, and specificity for the biomarker panels, logistic regression, followed by ROC curve analysis was performed. The formulas, coefficients, and constants of algorithm were optimized by setting the appropriate outliers and various logistic regression models. This developed algorithm, beads pre-coupled with four biomarkers, and various buffers for assay were bundled into QPLEX™ Alz plus assay kit.

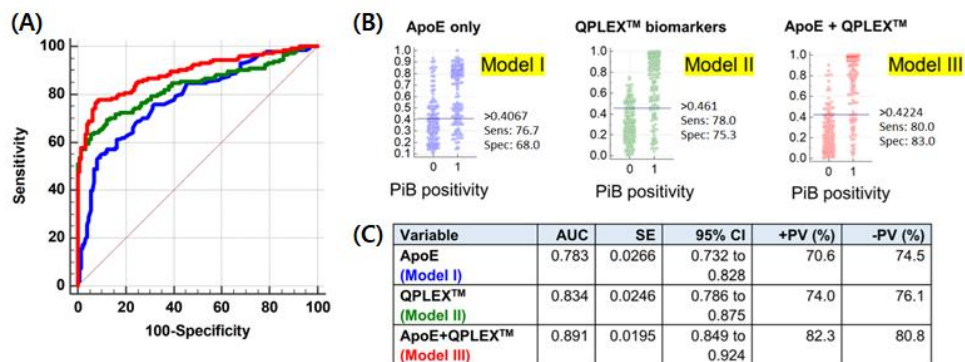


Figure 30. Receiver operating characteristic (ROC) curve analysis for PiB positivity. (A) ROC curve analyses for PiB positivity. Age and sex were used as covariates. (B) Interactive dot diagram and plot versus criterion values showing sensitivity, specificity, and Youden index cutoff criteria. (C) Comparison of ROC curve analyses. Age sex were used as covariates. Model III had the highest area under curve (AUC) value (0.891) [51].

Figure 30 shows performance of QPLEX™ kit. Three regression models (apolipoprotein E (ApoE) variable only, model I; QPLEX™ markers only, model II; ApoE + QPLEX™ markers, model III) were compared. Model II showed a higher AUC (0.834 with 76.6% sensitivity and 73.5% specificity) than model I (0.783 with 76.7% sensitivity and 68.0% specificity), and model III showed a significantly higher AUC (0.891 with 80.0% sensitivity and 83.0% specificity). The ApoE genotype currently stands as the strongest known risk factor for late-onset AD[62], but this genetic risk

factor does not reflect the risk an aging individual acquires related to the accumulation of life pattern– and environment–related factors. In contrast, the biomarkers assessed in the QPLEX™ Alz plus assay kit represent a real–time risk assessment for the initiation and progression of AD pathology. The results of ROC curve analysis revealed that the AUC value of the QPLEX™ Alz plus assay kit was higher than that of ApoE alone. Also, the combined screening of ApoE and blood biomarkers can be used to improve disease diagnosis. This result is comparable or superior to those from other tests using well–known plasma AD biomarkers such as plasma Aβ 42/40 ratio, Aβ 40/42 ratio, or plasma phosphorylated–tau (p–tau) [61,63–70].

▪ 식약처 인허가

시약	시험 장비 (QMIA)	시험 시약 (QPLEX™ Alz plus assay)
제조허가(신고) 번호	제외 제신 20-15호	제외 제허 20-589호
품목명	의료용광발광장치	면역화학검사시약
품목코드	J01060.01[1]	K02050.01[2]
제조사	쑤웬타매트릭스	

▪ 자동화 장비 Specification

Technologies	전자동 다중진단 플랫폼
샘플	blood(혈장)
TAT	3.5 시간
Throughput	23 샘플/run
Physical dimensions	- 1100mm (H) * 700mm (D) * 620mm (W) - 150 kg, 330 lbs



Figure 31. QPLEX™ Alz plus assay kit is approved by MFDS.

Based on above results[51], the QPLEX™ Alz plus assay kit was able to obtain the Ministry of Food and Drug Safety (MFDS) certification. Also, QuantaMatrix Immunoassay Automation (QMIA™) system was developed so that even non–expert experimenters could diagnose with this kit, and MFDS certification was also obtained. During this process, I can aware that there was another advantage of multiplex assay platform. For an algorithm that uses multiple biomarker results to qualify as an in vitro diagnostic device (IVD), the used biomarker results must also be from IVD–certified platforms and kits. If algorithm was developed using results from singlex platform such as ELISA, IVD certification must be obtained individually for each platform and kit. On the other hand, in algorithm using multiplex platform results, it can easily

prove that platform, kit, and algorithm each exist only one and are connected each other, so could obtain IVD certification at once.

3.3. Apply to the other independent cohort

The QPLEX™ Alz plus assay kit was verified in the other independent cohort named of Precision medicine platform for mild cognitive impairment based on Multi-omics Imaging Evidence-based R&BD (PREMIER, n=1,395). In previous study, amyloid beta deposition based on PET imaging and algorithm value of the kit were compared. Here, I checked relationship between QPLEX™ algorithm values and four clinically separated groups: CN, subjective cognitive decline (SCD), MCI, and AD. Also, the relationship between the algorithm values and groups divided by the scores of Mini-Mental State Examination (MMSE) and Clinical Dementia Rating (CDR) were explored. The MMSE is a screening tool that gives information about global cognition, and the CDR is a composite evaluation used mainly to determine the presence/absence of functional impairment. Finally, the relationship between the algorithm values and the subgroups fractionalized by demographic factors such as sex, age, or ApoE genotype were analyzed.

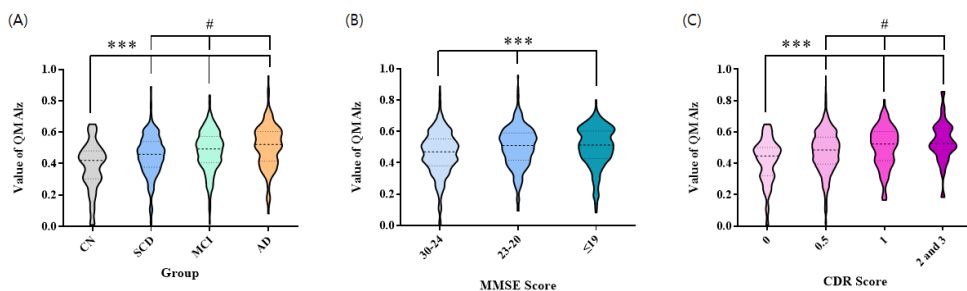


Figure 32. Difference of the QPLEX™ algorithm values among clinically separated groups, MMSE-separated or CDR-separated groups. The values of the QPLEX™ algorithm showed statistically significant differences among (A) four clinically separated groups, (B) MMSE-separated groups, and (C) CDR-separated groups.

I demonstrated that the QPLEX™ Alz plus assay kit could be a

useful tool for an early clinical diagnosis of AD. The QPLEX™ algorithm was developed for the purpose of determining the presence of cerebral amyloid deposition. Furthermore, I hypothesized that it can also be used to differentiate between CN and AD, based on the fact that statistically, CN has less amyloid deposition compared to AD. The results suggest that the kit can indeed distinguish the groups according to the clinical progression continuum of AD: CN, SCD, MCI, and AD (Figure 32A). Also, there was a significant difference in algorithm values between groups correlating with the score ranges of the MMSE or CDR (Figure 32B and C). These mean that the kit can distinguish among groups divided by the severity of dementia.

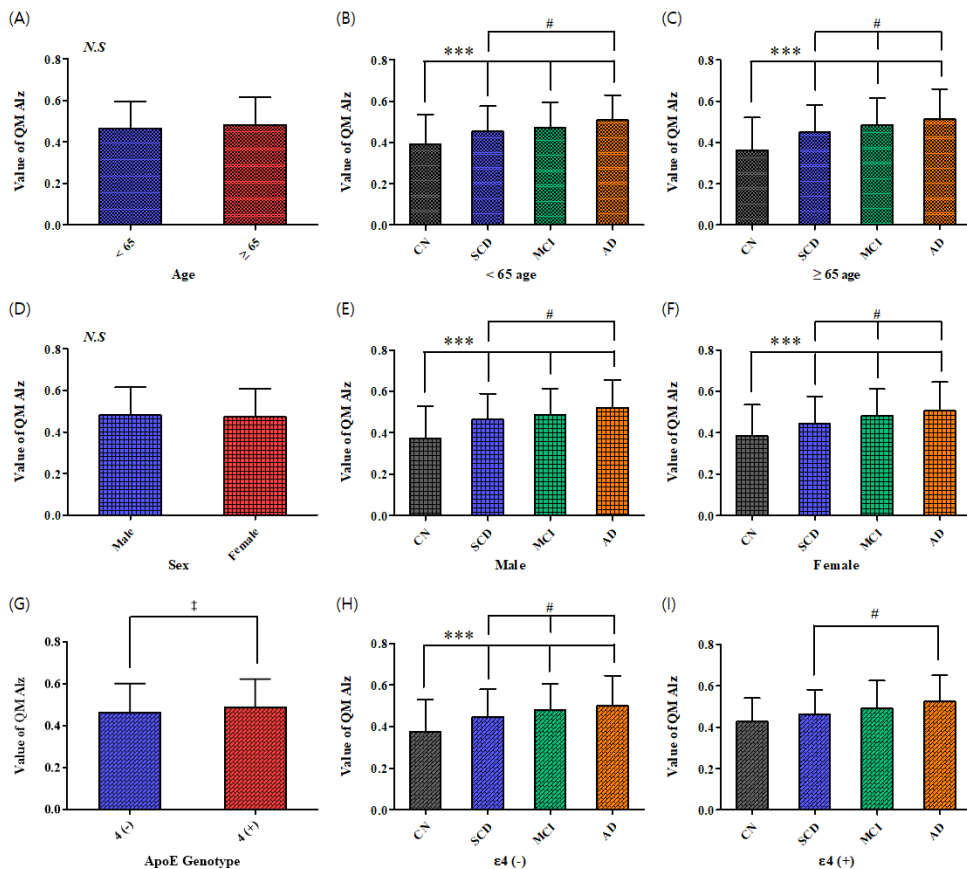


Figure 33. Difference of the QPLEX™ algorithm values within subdivided groups by various factors. (A) Comparison between groups under 65 and over 65. (B, C) Comparison among clinically separated subgroups by age. (D) Comparison between the male and female groups. (E, F) Comparison among clinically separated subgroups by sex. (G) Comparison between

ApoE ϵ 4 negative (ϵ 4 (-)) and ApoE ϵ 4 positive (ϵ 4 (+)) group. (H, I) Comparison among clinically separated subgroups by ApoE genotype.

For early diagnosis to be meaningful, it must also be valid for people under the age of 65. The correlation between algorithm values and clinical progress was present in patients above 65 years and below 65 years (Figure 33B and C). There were also significant algorithmic value differences between clinical progression in both males and females without bias (Figure 33E and F). This means that the kit can be used regardless of the age and sex of the patient. On the other hand, the presence or absence of the ApoE gene shows a significant difference in the QPLEX™ algorithm value (Figure 33G), because people with the ApoE gene are more likely to develop MCI or AD. As a result, the kit's accuracy is different depending on whether the patient has the ApoE gene (Figure 33H and I).

The QPLEX™ Alz plus assay kit, a multiplex system to analyze four blood biomarkers consisting of LGALS3BP, A β 40, ACE, and POSTN simultaneously, could be a useful tool for screening AD. In particular, the kit could be a useful detection tool for an early clinical diagnosis of AD, i.e., for SCD or MCI. The results also indicated a possibility that the kit could be a helpful diagnostic tool for cognitive impairments at health checkups because the kit can measure multiple blood biomarkers using only tens of microliters of blood.

3.4. Improvement of the kit using additional biomarker

In Figure 32A, although statistically there is significant difference between each group, there is considerable overlap in algorithm value even between CN and AD. It seems that due to application of different cohort from cohort used to develop algorithm and increase in number of participants by more than 4 times, insufficient performance of kit was revealed.

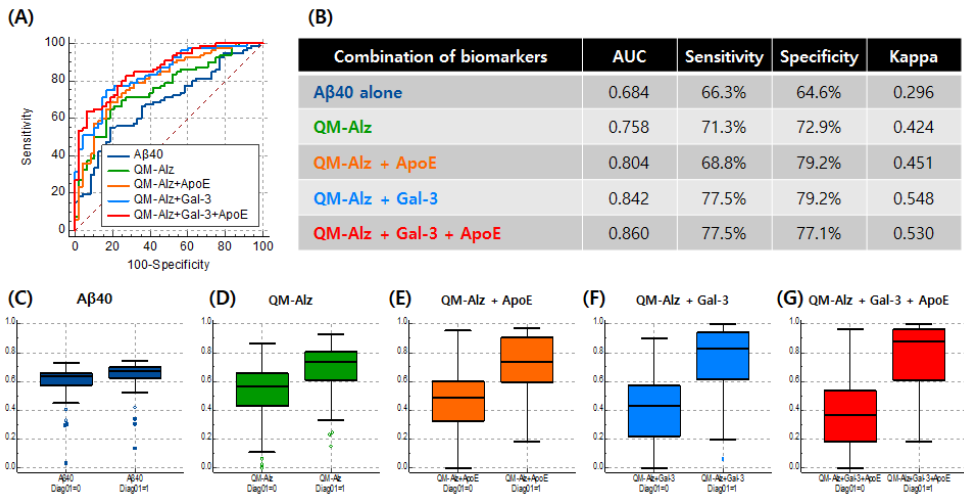


Figure 34. Various statistical analysis results for each biomarker combination. (A) Comparative ROC curves. (B) AUC, sensitivity, specificity, and kappa value. (C) to (G) Data comparison graphs for each biomarker combination.

I am developing the other kit introducing additional biomarker to improve insufficient performance of kit, and Figure 34 summarizes intermediate result of AUC, sensitivity, specificity, and kappa values according to the inclusion of additional biomarkers, galectin-3, in 546 samples of CN or AD among the PREMIER cohort. Overall accuracy has significantly increased. Especially, while there was considerable overlap between CN and AD in original QPLEX™ algorithm value (Figure 34D), overlap between CN and AD decreases considerably when galectin-3 is added (Figure 34F). One advantage of multiplex platform is that it is easy to add biomarkers. So performance can be easily improved by introducing explored biomarkers.

Chapter 4. Conclusion and Discussion

In this chapter, the proposed platform will be summarized. Then, the platform will be compared with the other commercialized platforms in the aspect of multiplex capacity, throughput, assay time, and applicable target. Also, the limit of this platform will be described. Finally, future works that can improve the platform will be presented.

4.1. Summary of dissertation

In this dissertation, I described the importance and need for multiplex assay platform. ELISA has long been used for biomarker detection in diverse body fluids, including blood and CSF, however, it requires intensive labor and typically shows intra- and inter-assay variability [9]. The bead-based multiplex assay platform uses a proprietary bead technology to perform 5,000 reactions in a single well. The bead is formed of a polymer that comprises a large amount of beads applied by a semiconductor process, and can easily be formed into various shapes [19]. The bead is further coated with silica to improve its physical and chemical stability, and to facilitate various chemical surface treatments [18].

However, although proof of concept was well established, it was not possible to apply to real diagnosis due to problems such as production capacity, instability of bead functionalization, lack of analysis equipment and decoding program, and lack of magnetism required for automation. To solve these problems, I developed a protocol to mass produce superparamagnetic nanoparticles, set up to photo-polymerize large quantities of beads, stabilized functionalization of bead surface, developed decoding program, and developed statistical analysis algorithm that represents probability of disease possession by combining multiple biomarkers. This platform was developed under the supervision of Quantamatrix Inc., so it was named as Quantamatrix multiplex assay platform (QMAP™).

Next QMAP™ was applied to various applications, and I described application to AD diagnosis as one of applications. Four biomarkers ($A\beta$ 40, LGALS3BP, ACE, and POSTN) excavated by *Park et al* [60,61] were quantified using QMAP™ and algorithm QPLEX™ Alz plus assay kit was developed using quantification results [51]. The kit showed higher performance than ApoE genotype currently stands as the strongest known risk factor for late-onset AD [62] and comparable or superior to those from other

tests using well-known plasma AD biomarkers such as plasma A β 42/40 ratio A β 40/42 ratio or plasma phosphorylated-tau (p-tau) [61,63–70]. Based on these results, the QPLEX™ Alz plus assay kit was received MFDS certification. Although somewhat insufficient performance was shown in process of evaluating kit in independent cohort, performance of kit is being improved by adding galectin-3 as an additional biomarker proven effective for AD diagnosis.

4.2. Comparison with the other commercialized technology

	ELLA	VERIGENE	FILMARRAY	LUMINEX	QMAP
Technique	Microfluidics	Microarray	Microarray	Bead	Bead
Target	Protein	Gene	Gene	Gene & protein	Gene & protein
Multiplex	1, 4	9 (extendable)	14 ~ 27 (extendable)	100 (extendable)	122 (extendable)
Instrument	\$90,000	\$40,000	\$60,000	\$40,000	\$40,000
Price of kit	\$150 ~ \$250	\$80 ~ \$160	\$155	\$80	\$80
Throughput	16, 32	1	1	96	96
Assay time	Hands on: 15m TAT: 2~3h	Hands on: 5m TAT: 2h	Hands on: 2m TAT: 1.5h	Hands on: 20m TAT: 3~5h	Hands on: 20m TAT: 1~3h

Table 6. Comparison of spec for with the other commercialized platform [71].

Table 8 summarizes specifications of commercialized multiplex assay platforms [71]. Although various platforms have been developed for multiplex diagnosis, the advantages of an encoded bead-based platform are clear in terms of implementable plex number, throughput, and ability to apply in both DNA and protein. Although there is a disadvantage that hands-on time is long, it was compensated by developing automation system.

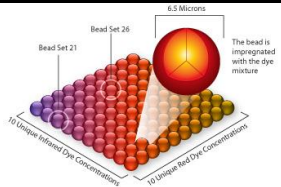


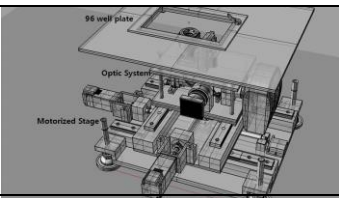
	Luminex	QMAP
Bead image		
Coding method	Combination of fluorescence dye	Shape
Stability of code	Code can be changed by light or heat	Code can be changed by physical damage
Reporter fluorescence	Wavelengths used for encoding are not available	Unlimited
Instrument image		
Analysis mechanism	Flow cytometry	Microscope with automated stage
Maintenance	Continuous and thorough maintenance is necessary	No special maintenance is required

Table 7. Comparison in principle between Luminex and QMAP™ [72].

The biggest competitor in bead-based multiplex platform is Luminex. In Luminex platform, microspheres of designated colors are coated with antibodies of defined binding specificities. Results can be read by flow cytometry because beads are distinguishable by fluorescent signature. Number of analytes measured is determined by number of different bead colors [72]. However, code of Luminex beads are affected by light and heat, and code may be altered. Also since fluorescence dye is already used during encoding process, there is limitation on type of fluorescence that can be used as reporter material. The biggest problem with Luminex platform is difficulty in maintaining analysis equipment. Since it uses flow cytometry, it is very important to keep flow channel clean. However, assay buffer contains a lot of salt and debris, so even if cleaning and maintenance are performed according to provided protocol, equipment failure rate is still high.

QMAP™ is free from these disadvantages of Luminex platform.

Graphical code is more stable than fluorescence code which can be affected by light and heat. Even if bead is damaged due to physical impact, almost all are filtered out by decoding algorithm. As a result, misrecognition rate is only 0.5% which can be completely removed by outlier removal algorithm. Maintenance of QMAP™ analysis equipment is also very convenient. Since it is simply a combination of fluorescent microscope and motorized stage, special management procedure is not required after initial calibration.

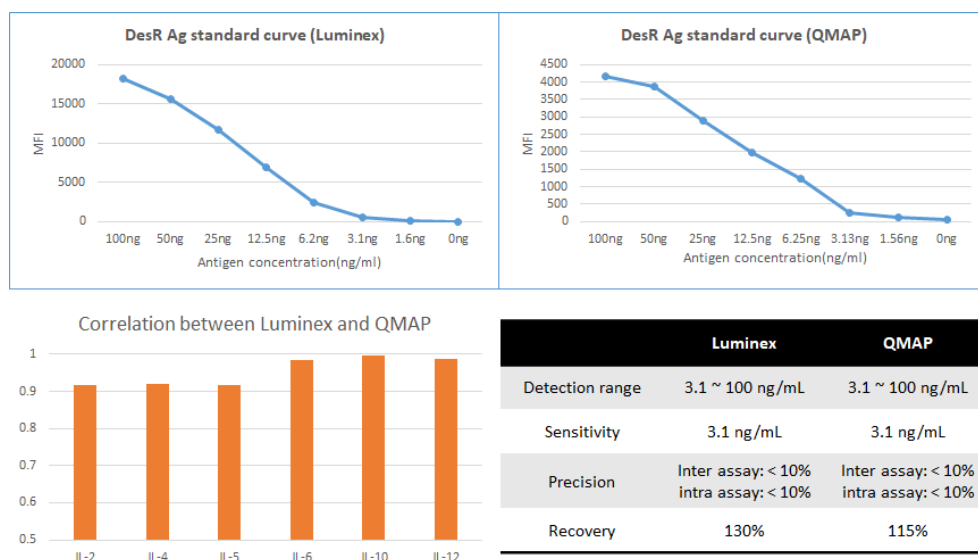


Figure 35. Comparison in assay performance between QM and Luminex with same antibody and antigen set.

In terms of assay performance, QMAP™ and Luminex showed the similar performance. When testing the same antigen–antibody pair in both QMAP™ and Luminex, they showed similar results in standard curve, detection range, sensitivity, CV in repeated experiments, and correlation for the same sample (Figure 35).

4.3. Limit of the platform

50um size bead sinks quickly in solution. This requires user' s skill. This is not a problem if QMIA™ is used, but QMIA™ consists of multiple modules so it is an expensive equipment that almost reaches \$100,000. To facilitate handling of QMAP™ bead, its size

needs to be reduced further. Especially, since there are no applications over 100-plex due to MRD problem, coding capacity does not need to be increased any further, there are no hurdles to reduce the size of bead.

One reason why it is difficult to find applications over 100-plex is the difference in MRD. Blood contains various substances, so some component existing in large amount in blood may inhibit antigen-antibody reaction desired by tester. If blood is diluted, concentration of target biomarker also decreases but concentration of inhibitor also decreases. Since affinity with probe is overwhelmingly on biomarker side, only antigen-antibody reaction occurs. Minimum dilution concentration required for this state is called MRD. Since various biomarkers have various concentrations and affinities in blood, each biomarker's MRD varies greatly. The MRD difference can be partially resolved through adjustment of assay buffer and comparison of multiple antibodies. However, if this MRD difference cannot be overcome, the advantage that QMAP™ can implement over 100-plex will be greatly reduced.

In molecular assay based on polymerase chain reaction (PCR) rather than immunoassay, high multiplicity of QMAP™ becomes great advantage. When QMAP™ was used for HPV, tuberculosis, and sepsis, 32-, 23-, and 36-plex were used for identification or drug resistance, respectively [46-49]. However, compared to real time (RT)-qPCR which completes handling just by putting sample and PCR mixture into PCR equipment, QMAP™ requires additional hybridization process after PCR. Especially, considering that multiplicity of RT-qPCR has been steadily improving, improvement in convenience of QMAP™ is needed. As one strategy, I am trying to perform PCR with primer-coupled beads. If PCR becomes possible in this way, each gene can be identified even without probe design as in RT-qPCR, and the difficulty of developing a PCR kit can be much lowered. In addition, although multiplicity is improving as technology advances, multiplexing in hundreds of units is impossible in RT-qPCR. If direct PCR is applied to the bead, it is anticipated to have a significant effect since QMAP™ already

possesses numerous codes. At present, the feasibility test has shown potential, and efforts are being made to enhance PCR efficiency.

4.4. Future works

As mentioned in limitation, bead size needs to be reduced further to improve handling. Especially, since there are no requirements over 100-plex, coding capacity does not need to be increased any further, so bead size can be reduced even more. To improve convenience of QMAP™ and follow trend in diagnosis field, sample-to-answer cartridge is being developed. If high plex encoded bead combines with cartridge platform, it can greatly outperform competing technologies. Currently, development of a cartridge platform for sepsis diagnosis is underway as an application.

As applications, the QMAP™ system was applied to HPV[46], tuberculosis[47,48], sepsis[49], and AD[50-52], and demonstrated excellent performance in all applications. Other application candidates that are expected to benefit by utilizing the multiplex characteristics of QMAP™ include prostate cancer, celiac disease, ovarian cancer, primary cancer detection, liver fibrosis, and sepsis. As introduced in the introduction, there are reports that accuracy has been increased by more than 30% by combining multiple biomarkers rather than using a single biomarker in prostate cancer and celiac disease[5,6]. *Bast RC Jr. et al.* reported that sensitivity was only 48% when using a single biomarker but sensitivity was increased to 75% by combining four biomarkers for early diagnosis of ovarian cancer[73]. *Kobayashi T. et al.* showed a diagnostic accuracy of about 85% by measuring about 20 biomarkers with ELISA while conducting research on primary cancer detection and recurrence prevention[74]. The sepsis kits base on molecular assay diagnose sepsis through the process of microbial culture, lysis, PCR, and QMAP™ assay. In contrast, *Harbarth S et al.* group

reported that sepsis can be diagnosed using blood biomarkers [75]. Sepsis is an inflammatory response due to microbial infection and is difficult to distinguish from inflammation due to other causes. *Harbarth S et al.* group showed that they could distinguish between other systemic inflammatory response syndrome and sepsis with 94% accuracy by combining three blood biomarkers. Most of the reports listed here measured each biomarker using ELISA method. If QMAP™ is applied to these applications, it is expected that the advantages of QMAP™ can be actively utilized.

Bibliography

- [1] A. M. Vicente, W. Ballensiefen J. I. Jonsson, How personalised medicine will transform healthcare by 2030: the ICPeMed vision, *J Transl Med* **18** (1) (2020). 180 <https://doi.org:10.1186/s12967-020-02316-w>
- [2] Y. F. Lu, D. B. Goldstein, M. Angrist G. Cavalleri, Personalized medicine and human genetic diversity, *Cold Spring Harb Perspect Med* **4** (9) (2014). a008581 <https://doi.org:10.1101/cshperspect.a008581>
- [3] A. A. McBride, Human papillomaviruses: diversity, infection and host interactions, *Nat Rev Microbiol* **20** (2) (2022). 95–108 <https://doi.org:10.1038/s41579-021-00617-5>
- [4] D. L. Robertson, B. H. Hahn P. M. Sharp, Recombination in AIDS viruses, *J Mol Evol* **40** (3) (1995). 249–259 <https://doi.org:10.1007/BF00163230>
- [5] J. F. Rusling, C. V. Kumar, J. S. Gutkind V. Patel, Measurement of biomarker proteins for point-of-care early detection and monitoring of cancer, *Analyst* **135** (10) (2010). 2496–2511 <https://doi.org:10.1039/c0an00204f>
- [6] S. D'Angelo, F. Mignone, C. Deantonio, *et al.*, Profiling celiac disease antibody repertoire, *Clin Immunol* **148** (1) (2013). 99–109 <https://doi.org:10.1016/j.clim.2013.04.009>
- [7] Wikipedia. *ELISA*, https://en.wikipedia.org/wiki/ELISA#cite_note-Schmidt2012-20
- [8] E. Engvall P. Perlmann, Enzyme-linked immunosorbent assay, Elisa. 3. Quantitation of specific antibodies by enzyme-labeled anti-immunoglobulin in antigen-coated tubes, *J Immunol* **109** (1) (1972). 129–135
- [9] N. S. Schoonenboom, C. Mulder, H. Vanderstichele, *et al.*, Effects of processing and storage conditions on amyloid beta (1–42) and tau concentrations in cerebrospinal fluid: implications for use in clinical practice, *Clin Chem* **51** (1) (2005). 189–195 <https://doi.org:10.1373/clinchem.2004.039735>
- [10] ProteinSimple, Ella Automated Immunoassay System,
- [11] Luminex. *The VERIGENE® System*, <https://www.luminexcorp.com/the-verigene-system/#overview>
- [12] Z. Xu, D. Chen, T. Li, *et al.*, Microfluidic space coding for multiplexed nucleic acid detection via CRISPR-Cas12a and recombinase polymerase amplification, *Nat Commun* **13** (1) (2022). 6480 <https://doi.org:10.1038/s41467-022-34086-y>
- [13] T. W. Chang, Binding of cells to matrixes of distinct antibodies coated on solid surface, *J Immunol Methods* **65** (1–2) (1983). 217–223 [https://doi.org:10.1016/0022-1759\(83\)90318-6](https://doi.org:10.1016/0022-1759(83)90318-6)

- [14] M. Schena, D. Shalon, R. W. Davis P. O. Brown, Quantitative monitoring of gene expression patterns with a complementary DNA microarray, *Science* **270** (5235) (1995). 467–470 <https://doi.org:10.1126/science.270.5235.467>
- [15] D. Wang, G. T. Carroll, N. J. Turro, *et al.*, Photogenerated glycan arrays identify immunogenic sugar moieties of *Bacillus anthracis* exosporium, *Proteomics* **7** (2) (2007). 180–184 <https://doi.org:10.1002/pmic.200600478>
- [16] I. Barbulovic–Nad, M. Lucente, Y. Sun, *et al.*, Bio–microarray fabrication techniques—a review, *Crit Rev Biotechnol* **26** (4) (2006). 237–259 <https://doi.org:10.1080/07388550600978358>
- [17] E. D. Dawson, L. R. Kuck, R. H. Blair, *et al.*, Multiplexed, microscale, microarray–based serological assay for antibodies against all human–relevant coronaviruses, *J Virol Methods* **291** (2021). 114111 <https://doi.org:10.1016/j.jviromet.2021.114111>
- [18] L. N. Kim, M. Kim, K. Jung, *et al.*, Shape–encoded silica microparticles for multiplexed bioassays, *Chem Commun (Camb)* **51** (60) (2015). 12130–12133 <https://doi.org:10.1039/c5cc02048d>
- [19] S. E. Chung, W. Park, H. Park, *et al.*, Optofluidic maskless lithography system for real–time synthesis of photopolymerized microstructures in microfluidic channels, *Applied Physics Letters* **91** (4) (2007). 041106 <https://doi.org:10.1063/1.2759988>
- [20] A. H. Lu, E. L. Salabas F. Schuth, Magnetic nanoparticles: synthesis, protection, functionalization, and application, *Angew Chem Int Ed Engl* **46** (8) (2007). 1222–1244 <https://doi.org:10.1002/anie.200602866>
- [21] J. Ge, Y. Hu, M. Biasini, W. P. Beyermann Y. Yin, Superparamagnetic magnetite colloidal nanocrystal clusters, *Angew Chem Int Ed Engl* **46** (23) (2007). 4342–4345 <https://doi.org:10.1002/anie.200700197>
- [22] S. Derveaux, B. G. Stubbe, K. Braeckmans, *et al.*, Synergism between particle–based multiplexing and microfluidics technologies may bring diagnostics closer to the patient, *Anal Bioanal Chem* **391** (7) (2008). 2453–2467 <https://doi.org:10.1007/s00216-008-2062-4>
- [23] D. C. Pregibon, M. Toner P. S. Doyle, Multifunctional encoded particles for high–throughput biomolecule analysis, *Science* **315** (5817) (2007). 1393–1396 <https://doi.org:10.1126/science.1134929>
- [24] H. Lee, J. Kim, H. Kim, J. Kim S. Kwon, Colour–barcoded magnetic microparticles for multiplexed bioassays, *Nat Mater* **9** (9) (2010). 745–749 <https://doi.org:10.1038/nmat2815>
- [25] D. N. Kim, W. Lee W. G. Koh, Micropatterning of proteins on the surface of three–dimensional poly(ethylene glycol) hydrogel microstructures, *Anal Chim Acta* **609** (1) (2008). 59–65 <https://doi.org:10.1016/j.aca.2007.12.024>
- [26] Z. Zhu, C. Wu, H. Liu, *et al.*, An aptamer cross–linked hydrogel as a

- colorimetric platform for visual detection, *Angew Chem Int Ed Engl* **49** (6) (2010). 1052–1056
<https://doi.org:10.1002/anie.200905570>
- [27] J. Kim, N. Singh L. A. Lyon, Label-free biosensing with hydrogel microlenses, *Angew Chem Int Ed Engl* **45** (9) (2006). 1446–1449
<https://doi.org:10.1002/anie.200503102>
- [28] H. Yin, Y. Ding, Y. Zhai, W. Tan X. Yin, Orthogonal programming of heterogeneous micro-mechano-environments and geometries in three-dimensional bio-stereolithography, *Nat Commun* **9** (1) (2018). 4096 <https://doi.org:10.1038/s41467-018-06685-1>
- [29] M. S. Shoichet, R. H. Li, M. L. White S. R. Winn, Stability of hydrogels used in cell encapsulation: An in vitro comparison of alginate and agarose, *Biotechnol Bioeng* **50** (4) (1996). 374–381
[https://doi.org:10.1002/\(SICI\)1097-0290\(19960520\)50:4<374::AID-BIT4>3.0.CO;2-I](https://doi.org:10.1002/(SICI)1097-0290(19960520)50:4<374::AID-BIT4>3.0.CO;2-I)
- [30] P. Haufova, Z. Knejzlik, J. Hanus, A. Zadrazil F. Stepanek, Reversible buckling and diffusion properties of silica-coated hydrogel particles, *J Colloid Interface Sci* **357** (1) (2011). 109–115 <https://doi.org:10.1016/j.jcis.2011.01.106>
- [31] S. W. Kim, Y. H. Bae T. Okano, Hydrogels: swelling, drug loading, and release, *Pharm Res* **9** (3) (1992). 283–290
<https://doi.org:10.1023/a:1015887213431>
- [32] S. L. Beaucage, Strategies in the preparation of DNA oligonucleotide arrays for diagnostic applications, *Curr Med Chem* **8** (10) (2001). 1213–1244
<https://doi.org:10.2174/0929867013372463>
- [33] M. Proupin-Perez, R. Cosstick, L. M. Liz-Marzan, V. Salgueirino-Maceira M. Brust, Studies on the attachment of DNA to silica-coated nanoparticles through a Diels-Alder reaction, *Nucleosides Nucleotides Nucleic Acids* **24** (5–7) (2005). 1075–1079
<https://doi.org:10.1081/ncn-200059170>
- [34] J. Ge Y. Yin, Magnetically Tunable Colloidal Photonic Structures in Alkanol Solutions, *Adv Mater* **20** (18) (2008). 3485–3491
<https://doi.org:10.1002/adma.200800657>
- [35] W. Stöber, A. Fink E. Bohn, Controlled growth of monodisperse silica spheres in the micron size range, *J Colloid Interface Sci* **26** (1) (1968). 62–69 [https://doi.org:10.1016/0021-9797\(68\)90272-5](https://doi.org:10.1016/0021-9797(68)90272-5)
- [36] B. M. Grommersch, J. Pant, S. P. Hopkins, M. J. Goudie H. Handa, Biotemplated Synthesis and Characterization of Mesoporous Nitric Oxide-Releasing Diatomaceous Earth Silica Particles, *ACS Appl Mater Interfaces* **10** (3) (2018). 2291–2301
<https://doi.org:10.1021/acsami.7b15967>
- [37] B. Bhushan, K. J. Kwak, S. Gupta S. C. Lee, Nanoscale adhesion, friction and wear studies of biomolecules on silane polymer-coated silica and alumina-based surfaces, *J R Soc Interface* **6** (37) (2009). 719–733 <https://doi.org:10.1098/rsif.2008.0398>
- [38] M. Sypabekova, A. Hagemann, D. Rho S. Kim, Review: 3–

- Aminopropyltriethoxysilane (APTES) Deposition Methods on Oxide Surfaces in Solution and Vapor Phases for Biosensing Applications, *Biosensors (Basel)* **13** (1) (2022). <https://doi.org:10.3390/bios13010036>
- [39] M. Zhu, M. Z. Lerum W. Chen, How to prepare reproducible, homogeneous, and hydrolytically stable aminosilane-derived layers on silica, *Langmuir* **28** (1) (2012). 416–423 <https://doi.org:10.1021/la203638g>
- [40] C. K. De, E. G. Klauber D. Seidel, Merging nucleophilic and hydrogen bonding catalysis: an anion binding approach to the kinetic resolution of amines, *J Am Chem Soc* **131** (47) (2009). 17060–17061 <https://doi.org:10.1021/ja9079435>
- [41] S. France, D. J. Guerin, S. J. Miller T. Lectka, Nucleophilic chiral amines as catalysts in asymmetric synthesis, *Chem Rev* **103** (8) (2003). 2985–3012 <https://doi.org:10.1021/cr020061a>
- [42] E. A. Smith W. Chen, How to prevent the loss of surface functionality derived from aminosilanes, *Langmuir* **24** (21) (2008). 12405–12409 <https://doi.org:10.1021/la802234x>
- [43] P. Bao, L. Zhang X. Wu, Canny edge detection enhancement by scale multiplication, *IEEE Trans Pattern Anal Mach Intell* **27** (9) (2005). 1485–1490 <https://doi.org:10.1109/TPAMI.2005.173>
- [44] ThermoFisher, Sulfo-NHS plus EDC (carbodiimide) crosslinking reaction scheme,
- [45] Bio-Rad. *Protocol: Sandwich ELISA with direct detection*, <<https://www.bio-rad-antibodies.com/sandwich-elisa-protocol-with-direct-detection.html>> (
- [46] Y. K. Lim, O. J. Kweon, J.-H. Choi, *et al.*, Analytical evaluation of a new Microdisk™ technology-based multiplex HPV genotyping system – the QPLEX™ HPV genotyping kit, *J Lab Med* **43** (4) (2019). <https://doi.org:10.1515/labmed-2019-0038>
- [47] H. Y. Wang, Y. Uh, S. Kim, T. S. Shim H. Lee, Evaluation of the Quantamatrix Multiplexed Assay Platform system for simultaneous detection of Mycobacterium tuberculosis and the rifampicin resistance gene using cultured mycobacteria, *Int J Infect Dis* **61** (2017). 107–113 <https://doi.org:10.1016/j.ijid.2017.06.008>
- [48] Y. Chang, S. Kim, Y. Kim, *et al.*, Evaluation of the QuantaMatrix Multiplexed Assay Platform for Molecular Diagnosis of Multidrug- and Extensively Drug-Resistant Tuberculosis Using Clinical Strains Isolated in Myanmar, *Ann Lab Med* **40** (2) (2020). 142–147 <https://doi.org:10.3343/alm.2020.40.2.142>
- [49] H. Y. Wang, Y. Uh, S. Kim H. Lee, Quantamatrix Multiplexed Assay Platform system for direct detection of bacteria and antibiotic resistance determinants in positive blood culture bottles, *Clin Microbiol Infect* **23** (5) (2017). 333 e331–333 e337 <https://doi.org:10.1016/j.cmi.2016.12.013>
- [50] D. Lee, J. C. Park, K. S. Jung, *et al.*, Application of QPLEX(TM) biomarkers in cognitively normal individuals across a broad age range and diverse regions with cerebral amyloid deposition, *Exp*

- Mol Med* **54** (1) (2022). 61–71 <https://doi.org:10.1038/s12276-021-00719-3>
- [51] J. C. Park, K. S. Jung, J. Kim, *et al.*, Performance of the QPLEX Alz plus assay, a novel multiplex kit for screening cerebral amyloid deposition, *Alzheimers Res Ther* **13** (1) (2021). 12 <https://doi.org:10.1186/s13195-020-00751-x>
- [52] H. J. Kim, J. C. Park, K. S. Jung, *et al.*, The clinical use of blood–test factors for Alzheimer's disease: improving the prediction of cerebral amyloid deposition by the QPLEX(TM) Alz plus assay kit, *Exp Mol Med* **53** (6) (2021). 1046–1054 <https://doi.org:10.1038/s12276-021-00638-3>
- [53] Y. Yoshiyama, V. M. Lee J. Q. Trojanowski, Therapeutic strategies for tau mediated neurodegeneration, *J Neurol Neurosurg Psychiatry* **84** (7) (2013). 784–795 <https://doi.org:10.1136/jnnp-2012-303144>
- [54] B. C. Uzuegbunam, D. Librizzi B. Hooshyar Yousefi, PET Radiopharmaceuticals for Alzheimer's Disease and Parkinson's Disease Diagnosis, the Current and Future Landscape, *Molecules* **25** (4) (2020). <https://doi.org:10.3390/molecules25040977>
- [55] R. A. Armstrong, beta–amyloid (Abeta) deposition in cognitively normal brain, dementia with Lewy bodies, and Alzheimer's disease: a study using principal components analysis, *Folia Neuropathol* **50** (2) (2012). 130–139
- [56] D. P. Salmon M. W. Bondi, Neuropsychological assessment of dementia, *Annu Rev Psychol* **60** (2009). 257–282 <https://doi.org:10.1146/annurev.psych.57.102904.190024>
- [57] H. Hampel, S. E. O'Bryant, J. L. Molinuevo, *et al.*, Blood–based biomarkers for Alzheimer disease: mapping the road to the clinic, *Nat Rev Neurol* **14** (11) (2018). 639–652 <https://doi.org:10.1038/s41582-018-0079-7>
- [58] K. Blennow H. Zetterberg, Understanding biomarkers of neurodegeneration: Ultrasensitive detection techniques pave the way for mechanistic understanding, *Nat Med* **21** (3) (2015). 217–219 <https://doi.org:10.1038/nm.3810>
- [59] S. E. O'Bryant, V. Gupta, K. Henriksen, *et al.*, Guidelines for the standardization of preanalytic variables for blood–based biomarker studies in Alzheimer's disease research, *Alzheimers Dement* **11** (5) (2015). 549–560 <https://doi.org:10.1016/j.jalz.2014.08.099>
- [60] J. C. Park, S. H. Han, H. Lee, *et al.*, Prognostic plasma protein panel for Abeta deposition in the brain in Alzheimer's disease, *Prog Neurobiol* **183** (2019). 101690 <https://doi.org:10.1016/j.pneurobio.2019.101690>
- [61] J. C. Park, S. H. Han, H. J. Cho, *et al.*, Chemically treated plasma Abeta is a potential blood–based biomarker for screening cerebral amyloid deposition, *Alzheimers Res Ther* **9** (1) (2017). 20 <https://doi.org:10.1186/s13195-017-0248-8>
- [62] C. C. Liu, C. C. Liu, T. Kanekiyo, H. Xu G. Bu, Apolipoprotein E and Alzheimer disease: risk, mechanisms and therapy, *Nat Rev Neurol*

- 9 (2) (2013). 106–118 <https://doi.org:10.1038/nrneurol.2012.263>
- [63] T. K. Karikari, T. A. Pascoal, N. J. Ashton, *et al.*, Blood phosphorylated tau 181 as a biomarker for Alzheimer's disease: a diagnostic performance and prediction modelling study using data from four prospective cohorts, *Lancet Neurol* **19** (5) (2020). 422–433 [https://doi.org:10.1016/S1474-4422\(20\)30071-5](https://doi.org:10.1016/S1474-4422(20)30071-5)
- [64] M. M. Mielke, C. E. Hagen, J. Xu, *et al.*, Plasma phospho-tau181 increases with Alzheimer's disease clinical severity and is associated with tau- and amyloid-positron emission tomography, *Alzheimers Dement* **14** (8) (2018). 989–997 <https://doi.org:10.1016/j.jalz.2018.02.013>
- [65] S. L. Risacher, N. Fandos, J. Romero, *et al.*, Plasma amyloid beta levels are associated with cerebral amyloid and tau deposition, *Alzheimers Dement (Amst)* **11** (2019). 510–519 <https://doi.org:10.1016/j.dadm.2019.05.007>
- [66] S. Palmqvist, S. Janelidze, E. Stomrud, *et al.*, Performance of Fully Automated Plasma Assays as Screening Tests for Alzheimer Disease-Related beta-Amyloid Status, *JAMA Neurol* **76** (9) (2019). 1060–1069 <https://doi.org:10.1001/jamaneurol.2019.1632>
- [67] V. Perez-Grijalba, J. Arbizu, J. Romero, *et al.*, Plasma Abeta42/40 ratio alone or combined with FDG-PET can accurately predict amyloid-PET positivity: a cross-sectional analysis from the AB255 Study, *Alzheimers Res Ther* **11** (1) (2019). 96 <https://doi.org:10.1186/s13195-019-0549-1>
- [68] A. Vergallo, L. Megret, S. Lista, *et al.*, Plasma amyloid beta 40/42 ratio predicts cerebral amyloidosis in cognitively normal individuals at risk for Alzheimer's disease, *Alzheimers Dement* **15** (6) (2019). 764–775 <https://doi.org:10.1016/j.jalz.2019.03.009>
- [69] A. Nakamura, N. Kaneko, V. L. Villemagne, *et al.*, High performance plasma amyloid-beta biomarkers for Alzheimer's disease, *Nature* **554** (7691) (2018). 249–254 <https://doi.org:10.1038/nature25456>
- [70] I. Feinkohl, C. G. Schipke, J. Kruppa, *et al.*, Plasma Amyloid Concentration in Alzheimer's Disease: Performance of a High-Throughput Amyloid Assay in Distinguishing Alzheimer's Disease Cases from Controls, *J Alzheimers Dis* **74** (4) (2020). 1285–1294 <https://doi.org:10.3233/JAD-200046>
- [71] M. J. Binnicker, Multiplex Molecular Panels for Diagnosis of Gastrointestinal Infection: Performance, Result Interpretation, and Cost-Effectiveness, *J Clin Microbiol* **53** (12) (2015). 3723–3728 <https://doi.org:10.1128/JCM.02103-15>
- [72] Luminex. <<https://www.luminexcorp.com/>> (
- [73] R. C. Bast, Jr., D. Badgwell, Z. Lu, *et al.*, New tumor markers: CA125 and beyond, *Int J Gynecol Cancer* **15** Suppl 3 (2005). 274–281 <https://doi.org:10.1111/j.1525-1438.2005.00441.x>
- [74] T. Kobayashi, A blood tumor marker combination assay produces high sensitivity and specificity for cancer according to the natural history, *Cancer Med* **7** (3) (2018). 549–556 <https://doi.org:10.1002/cam4.1275>

- [75] S. Harbarth, K. Holeckova, C. Froidevaux, *et al.*, Diagnostic value of procalcitonin, interleukin-6, and interleukin-8 in critically ill patients admitted with suspected sepsis, *Am J Respir Crit Care Med* **164** (3) (2001). 396–402
<https://doi.org:10.1164/ajrccm.164.3.2009052>

Abstract

드러난 증상이 같더라도 원인이 되는 질병은 다를 수 있다. 때문에 발현된 증상에 대하여 혈액, 객담, 소변과 같은 생체도래물질에 존재하는 바이오마커를 통한 진단이 많이 시행되고 있다. 기존 검사 방법인 효소 결합 면역 흡착 분석법(ELISA)과 같은 단일 분석 방법과 비교했을 때, 다중진단은 작업 흐름을 개선하고, 환자 샘플, 시약, 소모품, 검사 시간 등을 전반적으로 절약할 수 있다. 특히 환자 샘플의 사용량이 줄어든다는 점은 금전적 이익에 더하여 샘플 수집에 대한 부담을 줄임으로써 검사 접근성을 높일 수 있다는 장점이 있다. 또한 다수의 바이오마커를 조합함으로써 얻어지는 높은 정확도는 일상적인 검사를 통한 조기진단의 가능성을 높일 수 있다.

코드화된 미세입자를 활용한 다중진단 플랫폼에서는 미세입자에 부여된 코드에 따라 서로 다른 프로브를 붙이고, 수백 수천 개의 미세입자를 섞어서 환자 샘플과 반응시킨다. 환자 샘플과 반응이 이루어진 미세입자의 코드, 즉 프로브의 종류를 확인하면 환자의 바이오마커 정보를 알 수 있다. 해당 기술에 대한 개념에 대한 증명은 되어있었지만, 생산량의 부족, 생산 공정의 편차, 미세입자의 코드를 분석해줄 프로그램의 부재 등으로 인해 실제 진단시장에서 사용하기에는 부족한 상태였다. 본 논문에서는 코드화된 미세입자를 활용한 다중진단 플랫폼 기술을 실제 진단에 사용할 수 있는 수준으로 끌어올리는 개발과정을 기술하고, 개발한 플랫폼을 활용한 임상 결과 중 알츠하이머 치매에 적용한 결과를 서술한다.

생산 및 검사 과정에서 미세입자를 용이하게 다루고 반응의 편차를 줄이기 위해서는 미세입자에 자성을 부여해야 할 필요가 있다. 하지만, 상용 자성 입자는 외부 자력이 부재한 환경에서도 미세한 자력이 남아 있는 강자성 (ferromagnetic)을 띄고 있어 이를 활용할 경우 자성 입자들이 큰 덩어리를 형성함으로써 인해 미세입자의 형태를 균일하게 만

들 수 없었다. 이러한 문제를 해결하기 위해 외부 자력이 인가되었을 때만 자성을 띄고 외부 자력이 부재할 때는 자성이 사라지는 초상자성 (superparamagnetic) 나노 입자를 대량으로 합성하는 방법을 개발하였다.

원하는 형태로 패턴을 변경할 수 있는 micro-mirror-array에 반사된 자외선을 자외선에 의해 경화 (polymerization)가 되는 폴리머에 쏘아 줌으로써 원하는 형태로 미세입자를 생산할 수 있는 시스템이 개발이 되어 있었다. 미세입자의 형태를 실시간으로 다양하게 부여할 수 있다는 장점이 있는 시스템이었지만, 실제 진단 현장에서 미세입자를 활용하기 위해서는 수천만 개의 미세입자를 단 시간 내에 생산할 수 있는 시스템 개발이 필요하였다. 생산량을 끌어올리기 위해 반도체 공정에서 사용되는 대면적 노광 시스템을 도입하였고, 반도체에서 사용하는 photoresist와 폴리머의 차이로 인해 발생하는 문제들을 해결하여 시간당 생산량을 350만 개 이상으로 끌어올렸다.

미세입자에 바이오마커를 올리기 위해서는 적합한 작용기를 미세입자 표면에 만들어줘야 한다. 본 논문에서는 패턴 된 자외선으로 폴리머 입자의 형태를 만든 후, 실리카로 코팅하여 안정성을 높이고, 표면에 amine과 carboxylic acid를 순차적으로 올리는 방법을 고안하였다. 보편적으로 사용되는 APTES를 활용하여 amine처리를 하였을 때는 반응 과정의 무작위성 및 보관 과정에서의 가수분해로 인한 손실 문제로 인해 미세입자의 성능에 편차가 발생하였다. 이러한 문제를 해결하기 위해 대체 물질을 도입하고, 해당 물질의 특성을 활용하는 프로토콜을 개발하여 미세입자의 성능 편차를 5% 이하로 낮췄다.

수 um 크기의 미세입자에 효과적으로 코드를 부여할 수 있는 방법을 개발하였고, 이를 분석할 수 있는 자동 촬영 장비 및 코드 해석 알고리즘을 개발함으로써 코드화된 미세입자를 활용한 다중진단 플랫폼을 완성하였다.

개발한 플랫폼에 대하여 기존 검사 방법인 ELISA와의 비교평가를 수행하였다. ELISA에서는 매 검사 마다 프로브를 붙이는 작업이 필

요한 반면, 미세입자는 대량으로 프로브를 미리 붙여두고 장기간 사용할 수 있어 검사 준비 과정을 생략할 수 있었다. 한번의 검사에 필요한 프로브 물질의 양은 약 100배를 절약할 수 있었다. 10가지 바이오마커를 검사하는 것을 가정했을 때, 샘플의 양은 30배, 항체는 3배, 형광물질은 20배, 용매류는 15배 절약할 수 있었으며, 반응 시간도 절반으로 줄어들었다.

개발한 플랫폼은 자궁경부암, 성병, 결핵, 패혈증, 심혈관질환, 치매 등 다양한 임상에 활용되었으며, 본 논문에서는 해당 기술을 치매에 적용한 결과를 서술하였다. 치매는 임상적 증상이 발현하기 수십년 전부터 바이오마커에 변화가 일어난다. 이 바이오마커의 변화를 사전에 발견할 수 있다면 치료를 통해 치매의 발병을 유의미하게 늦출 수 있다. 기존에는 신경심리검사, 뇌척수액검사, PET 검사 등을 통해 치매를 진단하였는데, 신경심리검사는 조기진단이 불가능하고, 뇌척수액검사는 샘플 수집이 어려워 일상적인 검사에는 적합하지 않다. PET 검사 또한 비싼 검사비용으로 인해 접근성이 떨어진다. 본 논문에서는 혈액 내 여러 바이오마커를 측정하고 알고리즘화함으로써 약 80% 정확도로 치매 진단이 가능함을 보여주었다.

주요어: 다중진단, 코드화된 입자, 표면 작용기 처리, 이미지 프로세싱, 임상 적용, 치매

학번: 2013-30964